M.Sc. Thesis

# The shape of three dimensional bacterial colonies


UNIVERSITY OF COPENHAGEN

Martin Møller Larsen

# 3D colonies


| | |
|---|---|
| Author | Martin Møller Larsen |
| Supervisor | Assoc. Prof. Liselotte Jauffred |
| Supervisor | Assoc. Prof. Namiko Mitarai |



UNIVERSITY OF
COPENHAGEN

*Dissertation for the degree of Master of Science*


The Niels Bohr Institute



Submitted to the University of Copenhagen
April 1st, 2021

# Acknowledgements

I would like to thank my supervisors Liselotte Jauffred and Namiko Mitarai for their enthusiastic support and guidance. I would also like to thank everyone from the Experimental Biophysics group and the Biocomplexity group who have given me valuable input during the project.
A special thanks to my fellow master students Mireia Cordero Sánchez and Alba García Vázquez for their invaluable company and collaboration in the laboratory.
Finally i would like to thank my close family, my parents, older sister and brother-in-law for their support and love during what would otherwise have been a very lonely year.

# List of Abbreviations

RMS - Root Mean Square

CLSM - Confocal Laser Scanning Microscope

GLCM - Grey Level Cooccurrence Matrix

REL - WT REL606

AS - REL606mreB A53S

AK - REL606mreB A53K

GFP - Green Fluorescent Protein

ON - Over Night

ANOVA - Analysis Of Variance

# Abstract

Bacteria submerged in solid growth media can grow into three dimensional colonies. The Eden Growth model on a square lattice can model the growth of a three dimensional clustered in vitro grown 3D colonies can be imaged using Confocal Laser Scanning Microscopy. Colony morphology is influenced by both the surrounding environment of the colony and the growth properties of the individual cells making up the colony. In this thesis, using a combination of lattice computer simulation and in vitro experiments, it is shown that small fluctuations in colony environment has measurable effects on colony morphology that are much larger than the effect of individual bacterial cell shape.

# Contents

Chapter 1

# Introduction

Bacteria are biological cells, typically rod shaped, of a couple of micrometers in length. Being one of the oldest lifeforms on earth they inhabit a diverse range of environments such as water, soil, the human gut or the surface of a kitchen table. Bacteria can exist as single cells or in large aggregates known as colonies. Large colonies can originate from a single or few cells, when the bacteria grows by dividing into two genetically identical copies of itself. If this process is continued the colony will undergo exponential growth, until a time at which food recourse are depleted and growth stalls and the colony size saturates [1]. The phases of bacterial growth can be divided into four distinct phases: 1: The lag phase, the time from the bacteria is placed in an environment before they start growing. 2: The exponential phase where bacteria grows exponentially. 3. Stationary phase where bacteria dies at the same rate as they are growing often due to depletion of nutrients and 4. The death phase where cells in the colony dies at larger rates than they are growing due to a depletion of resources or due to an outside stress killing the bacteria [1]. This simple growth curve does not take into account the geometry of the colony, for large colonies competition for resources may be local, and colonies may spread out over areas where the nutrients available for the bacteria is non-uniform. Bacteria growing in solid media form compact three dimensional colonies and shall be the focus in this thesis.

The outline of this thesis will be to develop a protocol for growing bacteria inside solid medium such that a three dimensional colony can form. Then image grown bacterial colonies using Confocal Laser Scannig Microscopy CLSM in order to quantify the shape and texture of 3D colonies. In order to do so a set of parameters characterizing the shape, structure and surface of the colony will be introduced. Different bacterial strains grown on surfaces

has been shown to display a wide range of colony shapes and patterns [2] here the effect of cell morphology only on colony shape will be investigated by comparing bacterial strains that are identical genetically except for variation in cell shape. Comparison between grown and imaged 3D colonies and the Eden model will be made. The Eden model provides method for easily modelling 3D colonies by a simple to understand growth process of adding bacteria to the surface of a 3D colony [3], a theoretical framework for quantifying growth processes such as the Eden Model already exists by relating growth to a small set of scaling exponents. Modifications to the growth rules of the Eden Model will be made to explore colony shape and morphology phenomena observed experimentally.

# Chapter 2

# Theory

In this chapter the theoretical framework and known quantities of of the Eden model will be outlined. First explaining the process of Eden growth in section 2.1 and with this model as a basis introduce the scaling exponents that can be used to characterize a larger family of growth models in section 2.2. Expanding bacterial colonies can expect to encounter inhomogeneities in their growth conditions such as varying concentrations of nutrients or physical obstacles as they expand into new territory. A simple model for understanding the dynamics of bacterial fronts growing through an inhomogeneous environment will be introduced in section 2.3. In order to quantify real grown colonies confocal laser scanning microscopy, CLSM, will be used, in section 2.4 the basic concepts of CLSM from flourencence to imaging will be explained. From the 3D images provided by CLSM a set of parameters to quantify 3D bacterial colonies will established. With this theoretical framework to quantify and compare both real bacterial colonies and lattice modeling of bacterial growth will have been formulated.

## 2.1 Eden Model

The Eden model was first described by M. Eden to model the formation of cell colonies such as bacteria or the growth of cancer tumors[3]. The Eden model consists of adding cells to the surface of a stationary colony placed on a square lattice, with one bacteria each occupying a single site within the lattice. The cluster formed by adding sites to the surface of the cluster is called the aggregate [4].

### 2.1.1 Growth processes

Different versions of the Eden model exist [5] two of which shall be described here. In the first version, Version A, a seed is added in the center of a square lattice. The model then grows by the process of defining the surface as the set of unoccupied adjacent sites to the Eden cluster and selecting with equal probability one of the surface sites to occupy.
The other, Version B, defines the surface as the set of occupied sites in the Eden cluster with at least one adjacent unoccupied neighbor, one of the surface sites is then chosen equiprobably. One of the unoccupied adjacent neighbors is then chosen equiprobably and becomes occupied, this process is then iterated. A visual representation of Version A and B in 2D can be seen in figure2.1.

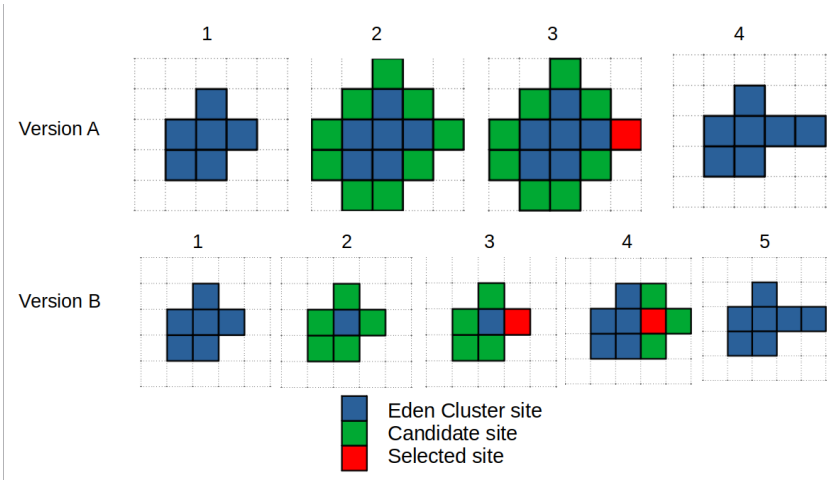


Figure 2.1: **Version A**: 1. The Eden cluster 2. The surface is defined as the adjacent unoccupied sites 3. One site is chosen equiprobably 4. The site becomes occupied. **Version B**: 1. The Eden cluster. 2. The surface is defined as the cluster sites with at least one unoccupied neighbor. 3. A surface site is chosen equiprobably 4. The candidate sites to grow to is the adjacent unoccupied sites 5. One of the candidate sites is chosen equiprobably

### 2.1.2 Anisotropy in the Eden model

For large Eden clusters of increasing size, the shape of the cluster is distorted away from a spherical shape into a diamond shape [6]. This distortion arises from the fact that each growth step from one site into another must happen along one of the lattice axes. This concept is not unique for Eden models and is seen in various other lattice models [4]. The anisotropy, $A_{\hat{x}}$, in a given direction, $\hat{x}$, can be measured by the ratio between the square distance from the center to the surface in the direction, $d_{\hat{x}}$, and the mean square distance

from the center to the surface which is just the radius of the Eden Model, R.

$$A_{\hat{x}} = \frac{d_{\hat{x}}}{R} \tag{2.1}$$

For the Eden model, the anisotropy has been shown to be 2% longer in the directions of the lattice. [6]

## 2.2 Scaling Exponents In Growth Models

The surfaces of growth models such as the Eden model can be characterized by a simple set of parameters describing the growth as a whole, they provide a method of comparing different growth models and determining if two models with differently formulated growth rules lead to the same types of clusters, models tat are similar in this way is called a universality class.

### 2.2.1 Flat Geometries

To introduce scaling exponents it can be useful to first consider a geometry where the Eden model grows upwards from a strip of seeds in 2D or in 3D from a plane of seeds. The height $h(i,t)$ of a single column $i$ at time $t$ is then simply the highest occupied site in that column and the average height $\bar{h}$ is the average height over all columns:

$$\bar{h}(t) = \frac{1}{L}\sum_{i=1}^{L} h(i,t), \tag{2.2}$$

Where L is the system size, ie. the number of columns. The width of the surface $\sigma$ is the Root-Mean-Square RMS of the surface height:

$$\sigma^2 = \frac{1}{L}\sum_{i=1}^{L}(h(i.t) - h(\bar{t}))^2 \tag{2.3}$$

As the model grows the width increases as a power of time [7]

$$\sigma(L,t) \sim t^{\beta} \tag{2.4}$$

Where $\beta$ is the growth exponent characterizing how the surface increases in roughness as time progresses. This roughening continues until a time $t_x$ where the width saturates at a value $w_{sat}$ the size of the saturation width is dependent on the systems sizes with the width scaling as a power of the system size [7]:

$$W_{sat}(L) \sim L^{\alpha} \tag{2.5}$$

Where $\alpha$ is the roughness exponent and characterizes the level of roughness at saturation. The time where saturation is reached also scales as a power of the system size [7]:

$$t_x \sim L^z \tag{2.6}$$

Where z is the dynamic exponent. The three scaling exponents are not independent, expressing the width in units of the saturation width and the time in terms of the saturation time:

$$\sigma \to \frac{\sigma(L,t)}{W_{sat(L)}}, t \to \frac{t}{t_x} \tag{2.7}$$

The scaling of $\frac{\sigma(L,t)}{W_{sat}(L)}$ becomes independent of system size, saturating at the characteristic time $\frac{t}{t_x}$. Now since scaling is independent of system size the scaling is only a function of time:

$$\frac{\sigma(L,t)}{W_{sat}(L)} \sim f\left(\frac{t}{t_x}\right) \tag{2.8}$$

$$\sigma(L,t) \sim L^{\alpha} f\left(\frac{t}{L^z}\right) \tag{2.9}$$

Where equation (2.9) is the Family-Vicsek scaling relation [7] Since on a log-log dividing $\sigma(L,t)$ with a constant $W_{sat}(L)$ only correspond to a shift in the curve:

$$log\left(\frac{\sigma(L,t)}{W_{sat}(L)}\right) = log\left(\sigma(L,t)\right) - log(W_{sat}(L)) \tag{2.10}$$

$\frac{\sigma(L,t)}{W_{sat}(L)}$ should still scale as a power law like equation 2.4 before saturation is reached:

$$\frac{\sigma(L,t)}{W_{sat}(L)} \sim u^{\beta} \quad u << 1 \tag{2.11}$$

Where $u = \frac{t}{t_x}$. Similarly the width should still saturate at some constant value. So the function $f(u)$ from equation 2.8 is characterized by two different scaling regimes:

$$f(u) \sim u^{\beta} \quad u << 1 \tag{2.12}$$

$$f(u) = \text{constant} \quad u >> 1 \tag{2.13}$$

For any growth process where equation 2.9 holds the scaling exponents can be related by considering that at time of saturation $t_x$ it should hold that

$$t_x^{\beta} \sim L^{\alpha} \tag{2.14}$$

$$t_x \sim L^{\frac{\alpha}{\beta}} \tag{2.15}$$

According to equation 2.6 the three exponents z, $\alpha$ and $\beta$ are related in the following way [7]:

$$z = \frac{\alpha}{\beta} \tag{2.16}$$

### 2.2.2 Radial Geometries

When growing the Eden model from a single seed at origin, the surface of the cluster is increasing at all times and the system size L increases as the model grow and we cannot simply consider the height at each column as when growing from a flat substrate, when calculating the width, $\sigma$, of the model. Instead, let $s$ be the set of surface sites within the cluster, the height of each surface site can be calculated as the radial distance from the center of the cluster, where both the center mass of the cluster and the origin can be considered the center of the cluster [8]. Let $\mathbf{x}$ be a surface site at time t, the height of the surface site $h(\mathbf{x}, t)$ is the radial distance to the origin then the width of the cluster is the RMS of all the surface heights in the cluster:

$$\sigma^2 = \frac{1}{N(s)} \sum_{\mathbf{x} \in s} (h(\mathbf{x}, t) - R)^2 \tag{2.17}$$

where $R$ is the radius of the cluster defined as the average surface height. Since the system size is increasing as the model grows,

$$L \to \infty, \text{ for } t \to \infty \tag{2.18}$$

there is no expected surface width where the model saturates [8] therefore the radial Eden cluster does not have a scaling exponent $\alpha$ and the only scaling parameter characterizing growth is the growth exponent $\beta$.:

$$\sigma \sim t^{\beta} \tag{2.19}$$

Where time is defined such that at each step in the model time increases as $\frac{1}{N(s)}$. With this definition of time, R scales linearly with time such that:

$$\sigma \sim R^{\beta} \tag{2.20}$$

For 3D radial geometries which will be the main focus in this thesis $\beta$ with respect to the origin has been found to be $\beta = 0.1047 \pm 0.0014$ [8].

### 2.2.3 Eden universality class

It can be shown that on short length scales version A and B gives different results. Continuing with the example cluster from figure 2.1, we can label the sites, the model can grow to in the following step with letters A - I as

| Site | A | B | C | D | E | F | G | H | I |
|---|---|---|---|---|---|---|---|---|---|
| $p_a$ | $\frac{1}{9}$ | $\frac{1}{9}$ | $\frac{1}{9}$ | $\frac{1}{9}$ | $\frac{1}{9}$ | $\frac{1}{9}$ | $\frac{1}{9}$ | $\frac{1}{9}$ | $\frac{1}{9}$ |
| $p_b$ | $\frac{2}{15}$ | $\frac{1}{15}$ | $\frac{1}{6}$ | $\frac{1}{10}$ | $\frac{1}{10}$ | $\frac{1}{10}$ | $\frac{1}{10}$ | $\frac{1}{6}$ | $\frac{1}{15}$ |

Figure 2.3: Table of probabilities that each of the adjacent sites is selected in for Eden model Version A $p_A$ and for Eden model version B $p_B$

shown in figure 2.2. Using the definitions of version A and version B of the Eden Model, the probabilities that each of the sites A - I becoming occupied in the Eden step in both version $p_A$ and $p_B$ can be calculated. These are shown in table 2.3. At large enough sizes however these differences does not effect scaling exponents in flat substrate geometries [5], meaning that both versions of Eden Growth gives the same scaling exponents and they belong to the same universality class.

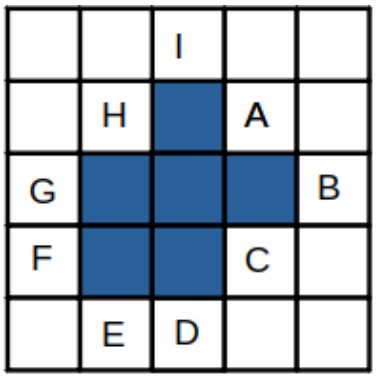


Figure 2.2: The adjacent sites of an Eden cluster in blue A - I, that can be chosen in the following step

## 2.3 The Growth Effect of Finite Sized Inhomogeneities

Bacterial colonies may undergo more complicated phases of growth where, growth along the colony is non uniform. In this section the effects of small inhomogeneities in the growth conditions of the colony will be considered, by considering a front propagating at constant speed normal to its own surface. Starting by considering the simple case of a front moving past a region where growth is not possible called an obstracle, the notion is extended to a part of the front moves through a region were growth speed is increased

### 2.3.1 Obstracles

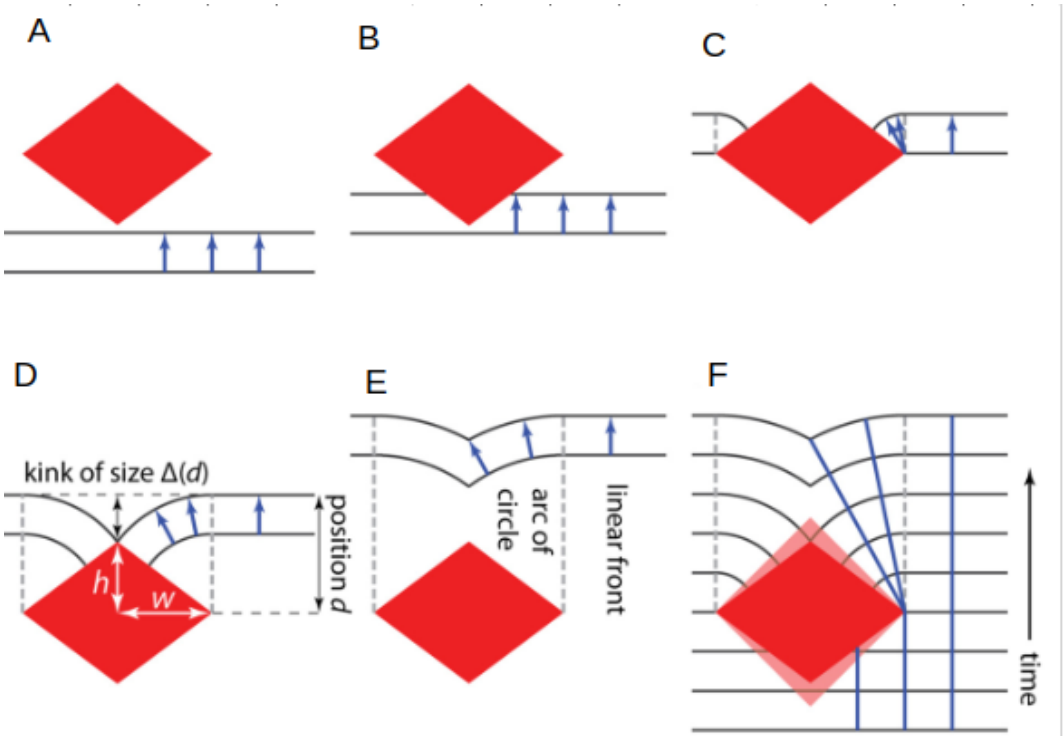


Figure 2.4: Constant Speed model. Modified from [9] fig 2. **A**: Front moves at constant speed. **B**: The front encounters a obstacle in red and is cutoff by it cutting the front in two. **C**: Beyond the widest points circular arcs normal to the obstacle are formed as the front moves at constant speed. **D**: Cicular arcs meet at the tip of the obstacle, forming a kink in the now reconnected front. **E**: The kink is then smoothed out as the radii of the circle elements continue to increase. **F**: Obstracles of similar widths w but diffrent heights h leaves the same kink in the front.

Define an obstacle to be a region in space where the bacterial colony cannot grow. Möbius, Murray and Nelson [9] proposes a constant speed model to quantify the effect of an obstacles on front shape as the colony grows around it. This model assumes that the front of the colony expands at constant speed normal to its surface ignoring the microscopic details of growth. The model is illustrated in fig 2.4 which shows a front moving at constant speed moving beyond a rhombus shaped obstacle.
The constant speed model predicts that beyond the widest points of the obstacle, circular arc connected between the linear part of the front and a point such that the circular arc hits the obstacle at a 90 degree angle will form. As the front moves with constant speed the two arc element should reconnect as the linear part of the front has moved a distance equal to the distance from

the widest point to the highest point of the obstacle along the surface of the obstacle beyond the widest point. For a rhombus shaped obstacle of height $2h$ and width $2d$ this distance $d$ is simply $d = \sqrt{w^2 + h^2}$. This form a kink of size $\Delta$ that then heals as the front moves forward, meaning that the size of the kink is a function of the distance traveled beyond the widest point of the obstacle $\Delta(d)$.
The size of the kink is given by distance between the height of the linear front $d$ and the height of the point of intersection between two circles with radius $d$ and centers located $2w$ apart. The intersecting point between two such circles is at $d\sqrt{1 - \frac{w^2}{d^2}}$, derived in Appendix A. Giving that the size of the kink $\Delta(d)$ is [9]:

$$\Delta(d) = d - d\sqrt{1 - \frac{w^2}{d^2}} \tag{2.21}$$

Expressed in unites of $w$

$$\frac{\Delta(d)}{w} = \frac{d}{w}(1 - \sqrt{1 - \frac{w^2}{d^2}}) \approx \frac{w}{2d} \quad d \ll w \tag{2.22}$$

Showing that the size of the kink is independent on the height of the obstacle $h$ and only the width of the obstacle determines the shape of the perturbation on the front caused by obstacle.

### 2.3.2 Hotspots

A hotspot is a small region in space where the growth rate $r_2$ of the bacteria located inside the hotspot is greater than than the growth rate outside of the hotspot $r_1$. The front dynamics caused by such a hotspot is shown in [10] to be described by applying the least time principle to the front moving through and beyond a hotspot, by considering the front at a given time to be the set of points whose path back to the initial condition of the growing front is traversed in the same amount of minimal time. The least of time principle is equivalent to the Eikonal Equation [10], that describes the arrival time to the front $T(\vec{x})$ to the as a function of the local front speed $v(\vec{x})$:

$$\left|\Delta T(\vec{x})\right| = \frac{1}{v(\vec{x})} \tag{2.23}$$

Where in a geometry with a hotspot, $v(\vec{x})$ is characterized by having two front speeds one inside the hotspot $v(\vec{x}_{in})$ and one outside the hotspot $v(\vec{x}_{out})$ where

$$v(\vec{x}_{in}) > v(\vec{x}_{out}) \tag{2.24}$$

Möbius et al [10] Found that hotspots half length $l$ causes a bulge in the front which is well described by a radial wave originating at the hotspot centre with radius given by

$$r = d + 2l(1 - \frac{r_2}{r_1}) \tag{2.25}$$

Where $d$ is the distance between the unperturbed part of the front and the centre of the Hotspot. Such a bulge is shown in figure 2.5. The bulge causes the area of effect of the hotspot to be an increasing parabola as the front moves beyond the hotspot. Where in a x,y reference system with origin in the centre of the hotspots and a front moving in the positive x direction, the area of influence from the hotspots is a sideways parabola described by the equation [10]:

$$y = \pm\sqrt{k^2 + 2kx} \tag{2.26}$$

With

$$k = 2l\left(1 - \frac{r_1}{r_2}\right) \tag{2.27}$$

The takeaway being that small hotspots with larger growth rates causes small bulges that spreads out sideways to the front causing a permanent perturbation on the shape of the front.

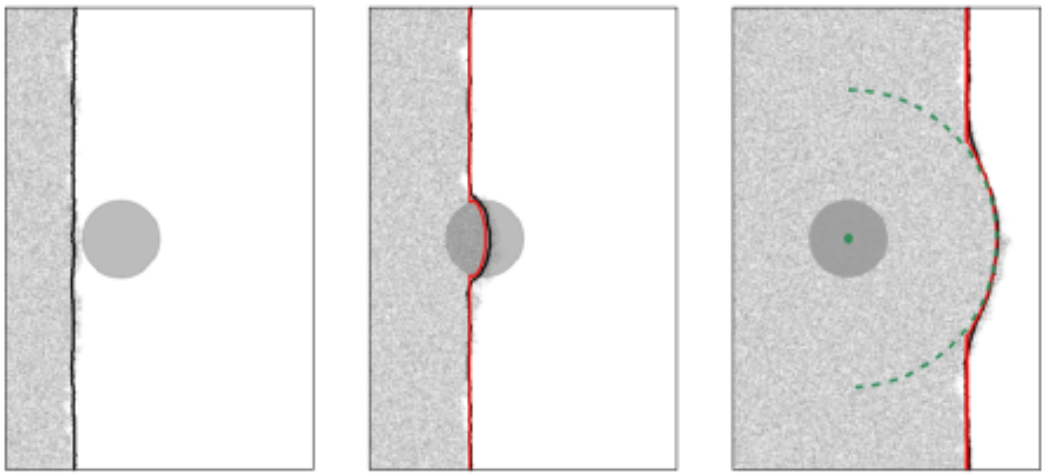

Figure 2.5: Bulge in the front caused by a hotspot. Figure from [10]

## 2.4 Imaging of Bacterial colonies

From growing 3D colonies to imaging to quantifying their structure, this section walk through the steps of explaining the how CLSM works by first introducing the concept of fluorescence that is used for imaging colonies and then defining a set of parameters that can be used to quantify the colonies imageed using CLSM

### 2.4.1 Fluorescence

Fluorescence is the process in which a fluorescent molecule reverts back to its ground state from an electronically exited state by emission of light [11]. The mechanism of fluorescence is shown in 2.6. The electric field of a light wave can excite electrons in its path from their ground state molecular orbital to a higher unoccupied molecular orbital. After absorbing energy from the excitation light the electron is in a higher vibrational state of its electronically exited state, it first relaxed by non radiative process to one of the lower vibrational sublevels of the first exited state. The electron the relaxes back it the ground state by emission of light, it is this emitted light that is called fluorescence.

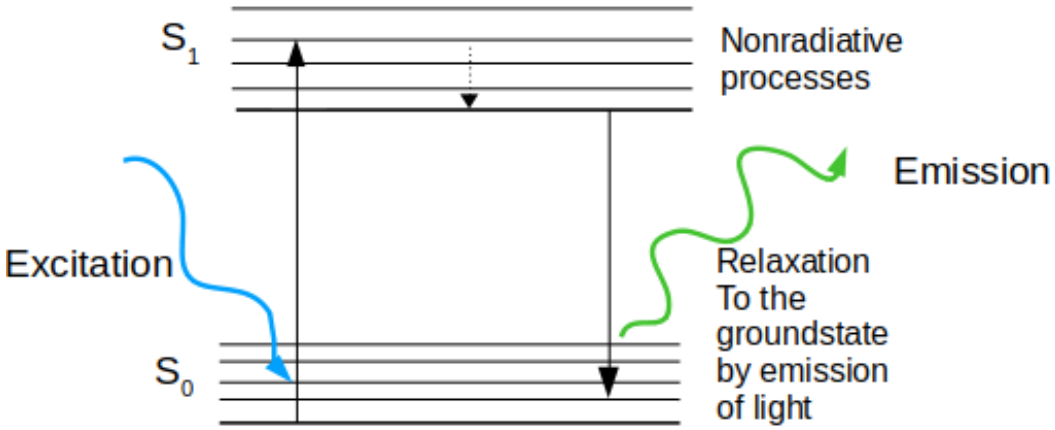


Figure 2.6: Concept of fluorescence. Light excites electron from ground state $S_0$ to a higher vibrational state of exited state $S_1$. Electron first relaxes to a lower vibrational sublevel of $S_1$, and then relaxes to the ground state emitting fluorescence light in the process.

Due to the dissipation of energy, when the electron relaxes to a lower vibrational sate in the first exited state, by non radiative processes. The energy of the emitted photon has a lower energy than the incident photon [11]. Since the energy of a light wave is:

$$E = \frac{hc}{\lambda} \tag{2.28}$$

where $h$ is planck constant, $c$ is the speed of light and $\lambda$ is the wavelength of the light. $\lambda$ of the emitted light is larger than the incident light. This is called the Stokes shift and allows for separation of the emission light from the excitation light, when using fluorescence for imaging.

### 2.4.2 Confocal Microscopy

Confocal Laser Scanning Microscopes (CLSM) allows for high contrast images of fluorescent light sources [12]. A schematic representation of how CLSM works is shown in 2.7. Laser light of an excitation wavelength is focused on a fluorescent sample, causing the fluorescent molecules to emit light of a longer wavelength than the excitation light allowing for filtering between the laser light and the emitted fluorescent light. Emission light passes through an objective lens and a pinhole lens through a small pinhole as seen in figure 2.7. This process causes light emitted from a small focal point in the sample to be the only light captured by the detector, as emission from above and below the focal point is blocked. Moving the focal plane pixel by pixel creating a 2D image. Scanning through a range of focal planes allows for the construction of a 3D image from the "z-stack" of 2D images.

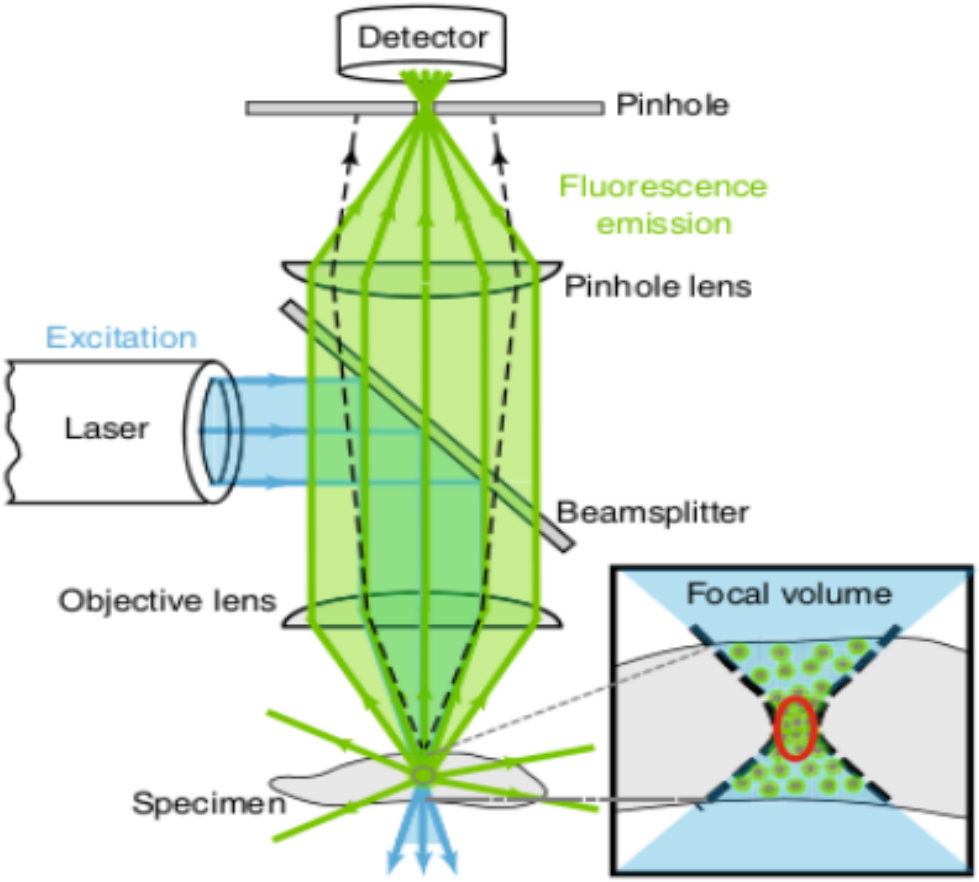


Figure 2.7: Schematics of CLSM [12]: Laser light excites the fluorescent sample. Light from only a small focal point in the sample passes through the pinhole to the detector, blocking out emission light from above and below the focal point

Selecting an objective lens provides a trade off between resolution and depth of Imaging, the objective lens is characterized by its magnification and numerical aperture, $NA$, which is defined as the half angle of the cone of light focused or collected by the objective, $\theta$, and the refractive index, $n$, of the mounting medium.

$$NA = nsin(\theta) \tag{2.29}$$

A larger $NA$ increases the resolution, from Rayleigh's criterion a rule of thumb for estimating the smallest features that can be resolved laterally [12] it can shown that a doubling in $NA$ results in a doubling of resolution.

$$R_{xy} = \frac{1.22\lambda}{2NA} \tag{2.30}$$

Where $\lambda$ is the wavelength of emitted light. However a higher $NA$ comes with the trade off of an increased $\theta$ decreasing the distance from the objective lens to the surface of the plate of the sample, which limits the depth at which the sample can be imaged into.

### 2.4.3 Quantifying 3D images

3D images captured by CLSM comes in the format of a stack of greyscale images with the X and Y directions along the 2D images and the layers of images being the Z direction, from these stacks Beyenal et al. [13] suggest a set of parameters to quantify morphology and shape of 3D biofilm, five of which shall be considered here, Aspect Ratio, Fractal Dimension, Textual Energy, Texutual Entropy, and Textual Homogeneity. The parameters Aspect Ratio and Fractal Dimension are calculated on binary images consisting of pixels belonging to the colony and background pixels. Therefore an appropriate threshold of the 3D greyscale image must be chosen, such that the surface morphology is preserved. Textual parameters Energy, Entropy and Homogeneity are calculated directly on 3D grey scale images.

#### Aspect Ratio

Aspect ratio measures the symmetry of the colony pixels in the $\langle X, Y \rangle$ direction. Thereby characterizing deviations away from spherical colony shapes. Aspect Ratio is calculated by measuring the run length in both X and Y direction, where a run length in the X direction is the amount of consecutive cluster pixels when walking along the X-direction of the image. Sweeping across the entire 3D image all run lengths in the X and Y direction can be averaged over giving the average run lengths in X and Y, AXRL and AYRL. The aspect ratio of a 3D image is then defined in [13] as:

$$\text{Aspect Ratio} = \frac{AXRL}{AYRL} \tag{2.31}$$

### Fractal Dimension

To introduce the concept of fractal dimension consider first some 1,2 and 3 dimensional nonfractal objects a line, a square and a cube as seen in figure 2.8. The line of length $l = 1$ can be split in to two copies of itself with half the length $l = \frac{1}{2}$, similarly a 2D square of length $l$ can be split into 4 copies of the original each one half the lengths of the original square. Finally a cube of length $l$ can be split into 8 copies of itself with each half the length of the original cube. A pattern arises where a shape of dimension D can be copied into $\frac{1}{2}^{-D}$ copies of itself when the length is halved. From this dimensionality D can be defined from how objects in that dimension scales in number of copies N with the length scale of the copies.

$$N \propto l^{-D} \tag{2.32}$$

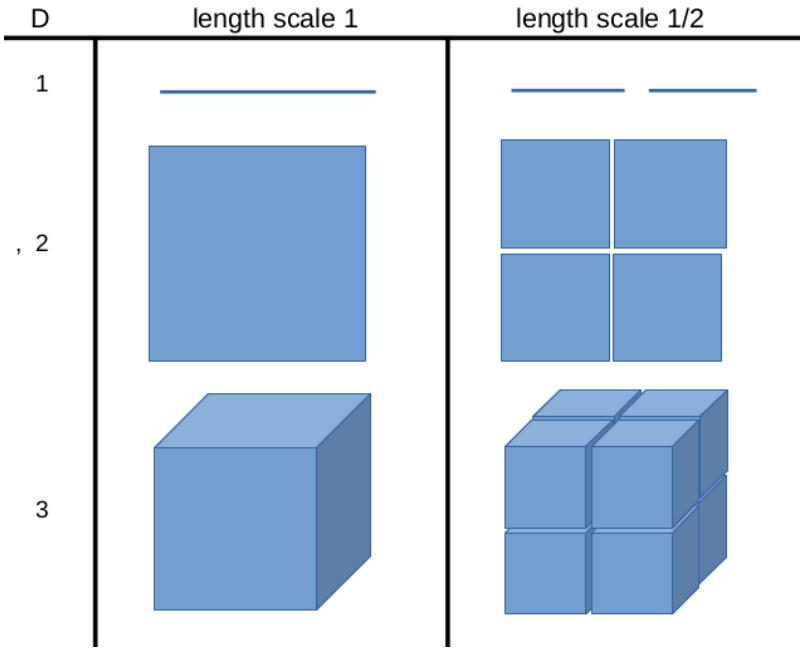


Figure 2.8: Objects of dimension D is made up of N smaller copies of themselves when the length scale $l$

This definition of dimension can be used to calculate the dimension of self-similar fractals such as the Sierpiński Gasket figure 2.9. It consists of 3 copies of itself with half the length, the dimension of the Sierpiński Gasket is therefore $D_f = -\frac{ln(3)}{ln(1/2)} = 1.5849$. The definition of fractal is any shape whose fractal dimension $D_f$ is smaller than the dimension its embedded in [14].

For non self-similar fractals to calculate the fractal dimension consider a box of linear size $l$ and count the number of boxes needed to cover the fractal. The fractal dimension is then

$$D_f = \lim_{l \to 0} \frac{ln(N(l))}{ln(1/l)} \tag{2.33}$$

For random fractals such as coastlines or surfaces of bacterial colonies the box counting method can be used to estimate the fractal dimension. The method consists of counting the number boxes needed to cover the fractal for different box sizes $l$. Plotting the values in a log-log plot a straight line can be fitted, the slope of this line is the fractal dimension $D_f$. Fractals embedded in 3D has fractal dimensions between 1 and 3 with higher fractal dimensions, meaning a more rough surface, where as a smaller fractal dimensions are more smooth surfaces [13].

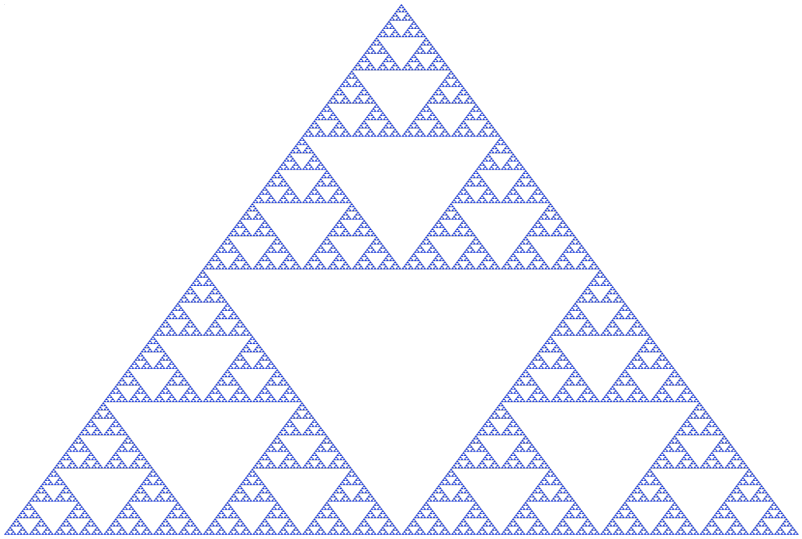

Figure 2.9: The Sierpiński gasket consisting of three copies of itself with half the length scale [15]

### Textual Parameters

The textual parameters analyzes the texture of a 3D greyscale image and describes the microscale heterogeneity of the colony by comparing the intensity, position and orientation of pixels [13]. Textual parameters can be calculated from the grey level co-occurrence matrix GLCM. GLCM is measure of the distribution of changes in grey level values between neighbouring pixels, it is calculated by counting how many times a pixel of value a is neighbours with a pixel of value b for all greyscale pixel values between 0 and 255, the defining a 256x256 Matrix $P_{XYZ}$ where the value at $P_{XYZ}(a, b)$ is the amount of times a pixel of value a is neighbours with a pixel of value b. Normalizing

by the the sum of all elements in $P_{XYZ}$ gives the GLCM $P_N(a,b)$

$$P_N(a,b) = \frac{1}{\sum P_{XYZ}} P_{XYZ}(a,b) \tag{2.34}$$

Where the (a,b) entry of the matrix contains the probability of a pixel of value $a$ being neighbours with a pixel of value $b$ [13]. From the GLCM the textual parameters can be calculated.

### Textual Energy

Textual energy can be calculated by summing over the square of the GLCM entries

$$\text{Energy} = \sum_{1}^{N_a} \sum_{1}^{N_b} P_N(a,b)^2 \tag{2.35}$$

Since energy increases as the square of the entries of the GLCM energy measures the regularity in the patterns of pixels. In a homogeneous image structure, there are a few dominant grey level transitions in the image, causing the GLCM matrix to have a few entries with large magnitude which will cause a larger energy measure compared to an more heterogeneous image, due to the entries being squared when summed.

### Textual Homogeneity

Textual Homogeneity can be calculated by summing the GLCM in the following way

$$\text{Homogeneity} = \sum_{1}^{N_a} \sum_{1}^{N_b} \frac{1}{1 + (a-b)^2} P_N(a,b) \tag{2.36}$$

Homogeneity is the sum of the GLCM entries scaled by the difference in intensity between neighbouring pixels, with a large grey level transition between neighbouring pixels contributing less to the homogeneity measure than neighbouring pixels with small differences in grey level values. Textual Homogeneity like Textual Energy is a measure of homogeneity in the image, but where Textual Energy measures the frequency in the patterns of pixels, Textual Homogeneity measures the similarity of spatially close image structures [13].

### Textual Entropy

Textual Entropy can be calculated from the GLCM in the following way

$$\text{Entropy} = -\sum_{1}^{N_a} \sum_{1}^{N_b} P_N(a,b) \ln(P_N(a,b)) \tag{2.37}$$

Entropy measures the randomness in the image. It is a measure of heterogeneity, a completly homogeneous images with only one pixel value across the entire image would have a entropy of 0 as $ln(1) = 0$. Entropy becomes large with many small entries in the GLCM as $ln(x) \to -\infty$ as $x \to 0$. Therefore Textual Entropy is a measure of heterogeneity within the image.

Chapter 3

# Experimental Materials and Methods

In this chapter the bacterial strains used to compare the effects of individual cell shape on colony shape is explained. Following this the protocol for growing bacterial colonies is established. In section 3.3 the image processing steps necessary to gain consistent and accurate results form the images produced by CLSM is discussed.

## 3.1 Materials

### Bacterial Strains

The three strains used to investigate the effect of cell shape on colony morphology is described in Monds et al. [16]. The three strains are genetically identical except for a single mutation in the genetic coding for the MreB protein, a prokaryotic actin homolog that is found in many rod-shaped bacteria and is thought to coordinate the spacial pattern of new material being inserted into the cell wall during rod-shaped elongation [16]. The wildtype strain used is the REL606 referred to as REL, and the two mutant strains of REL is REL606mreB A53S referred to as AS and REL606mreB A53K refered to as AK. The two mutant strains has growth rates a close to the ancestor REL strain, see figure 5C in [16] but differ in mean aspect ratio, with the REL having a mean aspect ratio of 4.44, AS having one of 3.55 and AK having one of 2.50. Phase contrast images of the 3 strains can be seen in 3.1 In all three strains the plasmid pmaxGFP (Amaxa/Lonza) [17] was introduced for detection of Green Fluorescent Protein with max excitation/max emission of $487nm/509nm$ by CLSM. The bacteria was grown on LB plates containing 1.5% agar, containing $50\mu g\ ml^{-1}$ in order to maintain their plasmids.

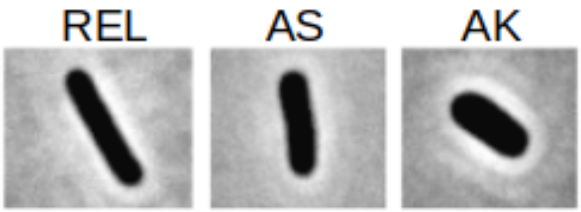


Figure 3.1: Phase Constrast of the strains from [16], showing the wildtype strain, REL, being a thin and long bacteria with a aspect ratio of approximately 4.4. AK being a shorter and wider bacteria of aspect ratio 2.50 and AS being intermediate between the two with an aspect raio of 3.55

**List of materials**

- Bacterial Strains REL, AS and AK with pmaxGFP plasmid
- 20 ml 0.625% agar + water
- Kanamysin antibiotics
- Minimal medium: 5x M63 salt, 1mg $ml^{-1}$ B1 stock solution, 1M Magnesium stock solution, 20 % wv glucose stock solution
- LB medium
- 2ml Eppendorf tubes
- 4.5 cm diameter glass bottom plates

## 3.2 Protocol for growing 3D colonies

Now a protocol for growing 3D colonies can be established, this protocol was used for all bacterial colonies grown and quantified in this thesis

### *3.2.1 Protocol*

**Step 1**

Grow the bacterial strains in 2 ml LB medium with 50 mg/ml kanamysin at 37° C for 8 hours.

**Step 2**

After 8 hours place 2 ml Eppendorf tubes in a heat bath at 55°C.

**Step 3**

Warm in microwave bottle of 20 ml 0.625% agar + water until the agar is fully melted

**Step 4**

When agar is melted add to the bottle: 5 ml 5x M63 salt, 25 $\mu l$ 1 mg/ml B1 stock solution, 50 $\mu l$ 1 M Magnesium stock solution, 250 $\mu l$ 20 % w/v glucose stock solution. Mix the solution.

**Step 5**

Quickly add 1.5 ml agar + minimal media solution to each of the Eppendorf tubes in the 55°C heatbath to keep the agar in a liquid state.

**Step 6**

Serially dilute the 10 $\mu l$ bacterial culture in 1ml LB medium 3 times and add from the final dilution 10 $\mu l$ bacterial culture to the agar + minimal media in the heat bath along with 50 mg/ml kanamysin. Such that the concentration of bacteria added to the Eppendorf tubes in the heat bath is $10^{-8}$ times the concentration over night culture. As shown in figure 3.2

**Step 7**

Pour the content of the Eppendorf tubes into glass bottom plates, and let it sit for 5 minutes to let the agar solidify. Place in incubator and let the colonies grow for 15 hours at 37°C.

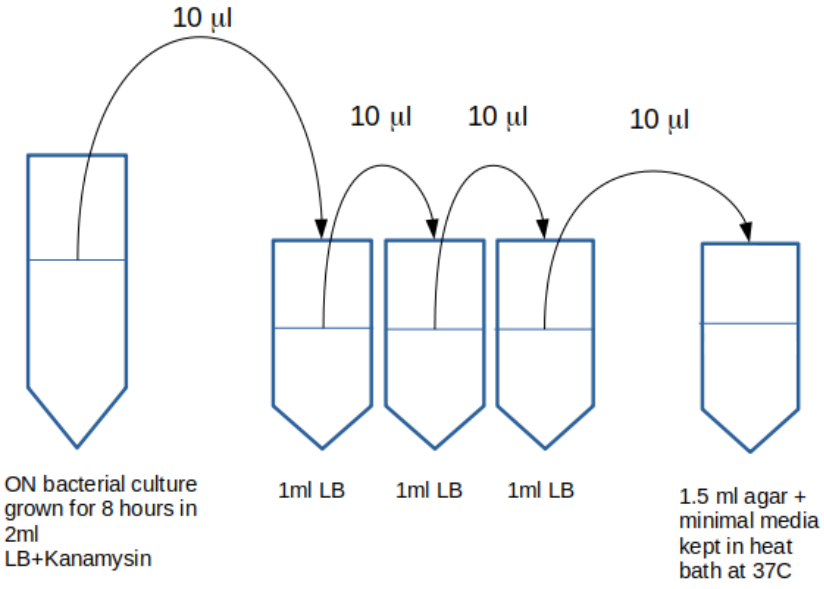


Figure 3.2: Serial dilution from step 6 of the protocol, ON culture is diluted such that the concentration of bacteria added to the minimal media + agar is $10^{-8}$ times the concentration in the ON culture

### 3.2.2 Optimizing colony count

Serial dilution was done with the aim of having on average 5-8 colonies pr. plate, 5-8 was chosen as the target colony count to avoid wasting time and resources on plates with 0 colonies due to random fluctuations in cell count during serial dilution and to prevent competition for nutrients between neighbouring colonies. This turned out to give colony counts of between 0 and 15+ colonies, due to both varying initial concentration of bacteria in the over night culture and each step in the serial dilution the concentration of bacteria the $10\mu l$ being Poisson distributed. To get more stable colony counts the concentration of bacteria in the ON culture was measured using measurements of the optical density. Using OD600 a method for measuring the density of a sample by passing light at 600nm through a sample and measuring the absorption of light coming out of the sample, the light passed into the sample will be scattered by the cells in the sample and this difference is measured by measuring the absorption of the light passed through the sample. The OD600 measure is then [18]:

$$\text{OD600} = A_{600} \cdot D \cdot c_f \tag{3.1}$$

Where $A_{600}$ is the absorbed light, $D$ is the dilution of the sample and $C_f$ is a correction factor for the used spectrometer. The concentration of cells pr ml is then a multiplier of the measured OD600, given by how many cells pr ml corresponds to OD600 = 1.0.
A serial dilution procedure was then calculated from the concentration of the overnight culture such that the expected cell count in one plates is 5. For example if the the OD600 measured cell density in an overnight culture is $2.5 \cdot 10^8$ cells pr ml, the expected number of colonies pr plate using the serial dilution shown in fig 3.2 would be 2-3 colonies, which with each step of the serial dilution being Poisson distributed has a much larger zero chance of having 0 colonies in the final plate $p \approx 8\%$. Instead the serial dilution could be modified by for example taking $25\mu l$ from the overnight culture in the first step of the dilution, resulting in the expected number of colonies to be 6-7 in the final plate and $p \approx 0.2\%$ chance of having 0 colonies.

## 3.3 Image Processing

CLSM was done on a Leica SP5 confocal microscope using a 488 nm excitation laser and samples were imaged using both a Leica N Plan L 40x/0.55na DRY objective and a HC PL APO 63x/1,20na W CORR CS2 [19] objective. Image processing was done in FIJI/IMAGEJ.

In CLSM imaging depth is limited by scattering and absorption of by the

emission and excitation light. As the focal point is moved deeper into the sample the excitation light has to penetrate through out of focus material, the intermediate material between the light source and the focal point will absorb and scatter an increasing amount of the excitation light. Similarly emission light has to pass through material to exit the sample and reach the detector leading to it being absorbed and scattered by the material between the focal point and the detector [20]. This leads, as shown in fig 3.3 showing the maximum intensity projection of the 3D colony in the XY and the YZ, to colonies with clearly imaged bottom halves and then features slowly fading as the focal point is placed further into the colony.

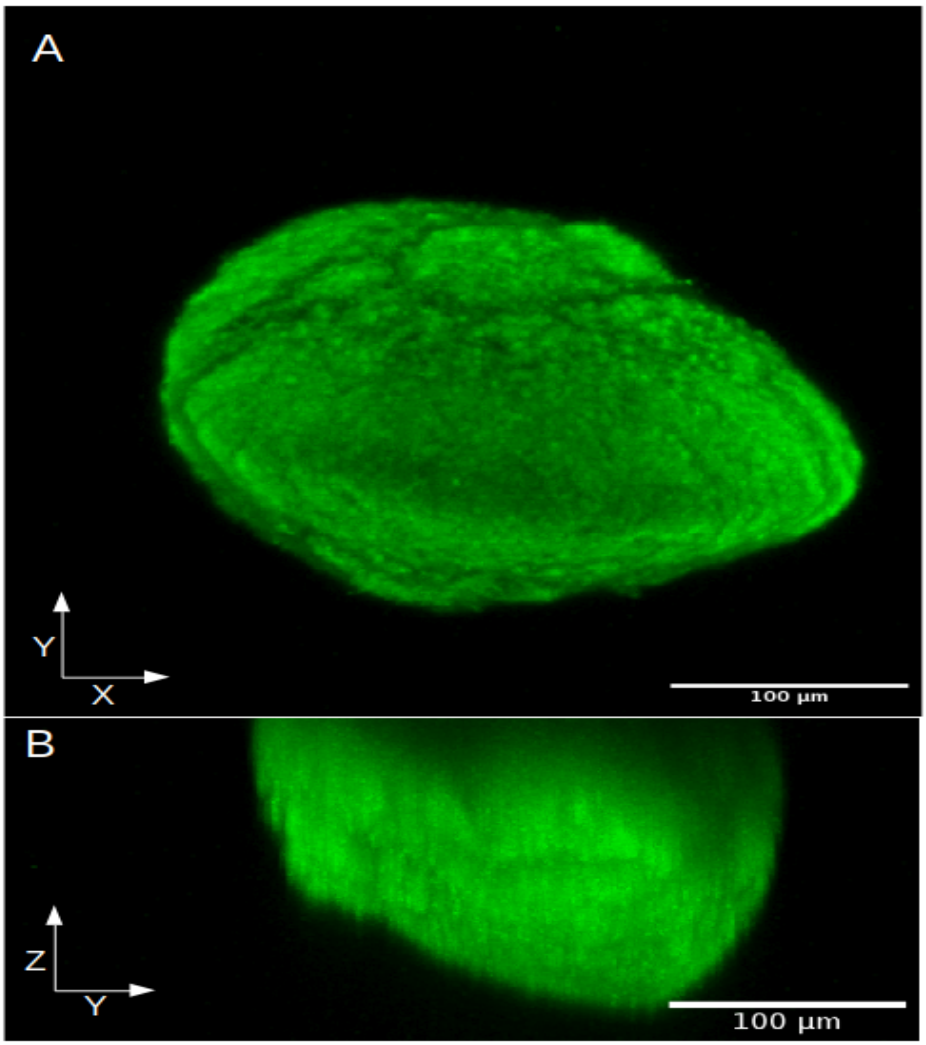


Figure 3.3: Image of REL strain type colony. Maximum intensity projection in the A) XY plane and B) YZ plane, show how the bottom surface of the colony is clearly images where as the colony is imaged deeper into the z direction the intensity stats to fade and continues as a shadow of the colony

Similarly as shown in fig 3.4 colonies ability to have any rotation in 3D space could cause different sections of the colony to start fading at different penetration depths. 3.4 A-B shows a REL colony seen from the $XZ$ direction in A and in B the same colony is shown rotated 180° in the $-XZ$ direction the side of the $XZ$ side of the colony stats to fade at a lower penetration depth than the $-XZ$ side of the colony. 3.4 C1-C3 shows an illustration of a oval shaped colony slightly tilted in the XZ plane, light is passed through the colony in C2 on the left hand side travels longer in the Z-direction before having to penetrate into the colony causing the left side of the colony in C3 to be imaged clearly at a focal plane marked by the red dashed line, while the right side of the colony scattering effects is causing poor resolution due to the light having to penetrate deeper through the colony to reach the red focal plane.

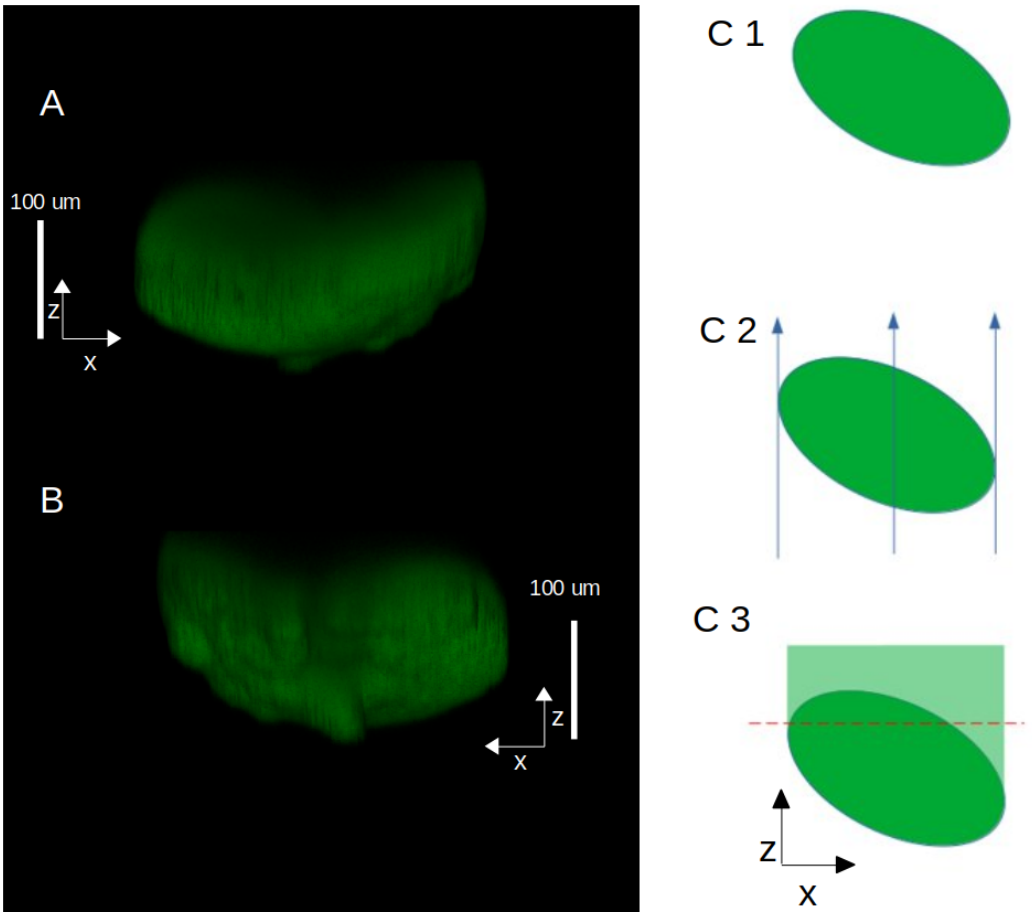


Figure 3.4: A-B: REL strain colony imaged from the XZ plane and the -XZ plane, showing diffrent resolutions and similar heights C1-C3: Illustration of tilted colony being imaged causes different penetration depths between right and left side of the colony at the same focal plane, which results in poorer resolution on the right side of the colony

Due to high resolution imaging depth only being available for one half of the colony a cutoff was chosen for each 3D image file. The Cutoff was chosen with the aim of keeping all of the surface structure of the imaged colony half. This was done manually for all images, a segmentation of all images was also done with manually chosen thresholds to preserve the surface structure of the colony. 3.5 shows the XZ projection of the REL strain colony shown before image processing and after threshold and cropping.

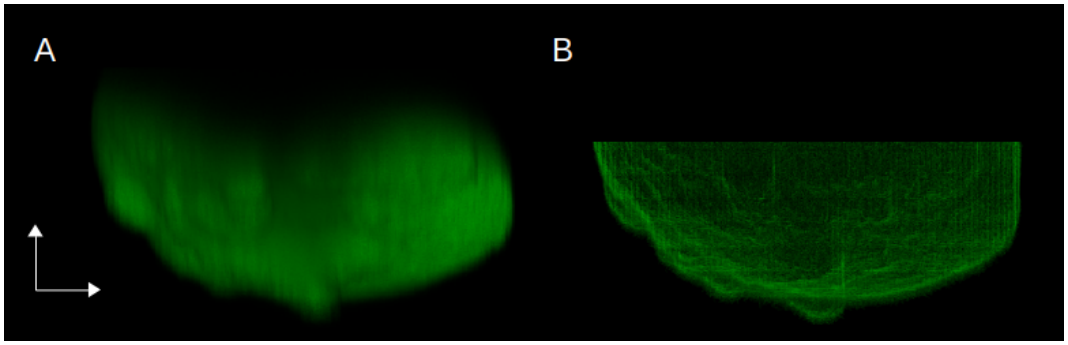


Figure 3.5: XZ projection of REL conlony A) Before image processing B) After Image processing

## 3.4 Statistical Analysis

Each of the parameters of colony shape and texture introduced in section 2.4.3. were measured on the 3D images taken with CLSM. For statistical analysis to compare differences in measured parameters between strain Analysis of Variance ANOVA were conducted.

ANOVA assumes samples to be Gaussian but of unknown variance. Having a total data set of N elements with mean $\bar{x}$ divided into N groups g, each with $N_g$ elements, where $N = \sum_g N_g$, mean $\bar{x}_g$ and variance $V_g$. Assuming a null hypothesis that the true mean of each group $\mu_g$, of which $\bar{x}_g$ is an estimate, are the same any differences in measured $\hat{x}_g$ between groups will only be caused be statistical fluctuations due to the true unknown standard deviation $\sigma$. $\sigma$ can be estimated by the variation within the groups. F-testing consists of comparing the variance within groups and between groups, if the variance between groups is significantly larger than variance within groups [21]. The F statistic is measured by calculating the sum of squares between groups divided by the degrees of freedoms $n - 1$ between groups

$$MSB = \frac{1}{n-1} \sum_g N_g (\bar{x}_g - \bar{x})^2 \tag{3.2}$$

and dividing it by the sum of squares within groups divided by the degrees of freedom within groups

$$MSW = \frac{1}{N-n} \sum_{g} \sum_{i \in g} (x_i - \bar{x}_g)^2 \tag{3.3}$$

From which the F statistic can be calculated

$$F = \frac{MSB}{MSW} \tag{3.4}$$

A large F statistic means that the variation between groups is larger than the variation within groups, the F statistic can be compered to an F-distribution to determine weather this difference is large enough. The null hypothesis that all groups are the same will be rejected if the chance of drawing a measured F-statistic from its F-distribution is less than $\alpha = 0.05$. Rejection of the null hypothesis means that at least one of the measured groups are significantly different from the others, to determine which t-test between groups were conducted to determine which individual groups were significantly different.

Chapter 4

# Experimental Results and Discussion

A data set consisting of 22 REL, 16 AS and 13 AK colonies was imaged with Leica N Plan L 40x/0.55na DRY objective [22] in order to analyse the colony shape, sizes and morphology with the parameters described in section 2.4.3, the full dataset is available online or ERDA [23]. Before analyzing the full dataset some observations about the morphology of the colonies is made using a subset of the colonies shown in figure 4.1, which shows a maximum intensity projection in the XY plane of 15 colonies 5 of each strain REL, AS and AK with each of the five colonies belonging to their respective strain coming from the same plate.

### Colony size

Using the maximum intensity projection the order of magnitude of bacteria in the colony can be estimated. The radius of the colonies is on the scale of $100\mu m$, assuming spherical colonies the volume of the colonies proportional to $r^3$ where r is the radius of the colonies giving a colony volume V of

$$V \propto (100\mu m)^3 = 10^6 \mu m^3 \tag{4.1}$$

Approximating the volume of a single E.coli cell to be $\sim 1\mu m^3$ as REL has a cell width of $0.72 \pm 0.01$ $\mu m$ and cell length of $3.06 \pm 0.04$ $\mu m$ [16]. The number of cells, N, in a single colony grown for 15 hours is on the order of millions of cells:

$$N \propto 10^6 \text{cells} \tag{4.2}$$

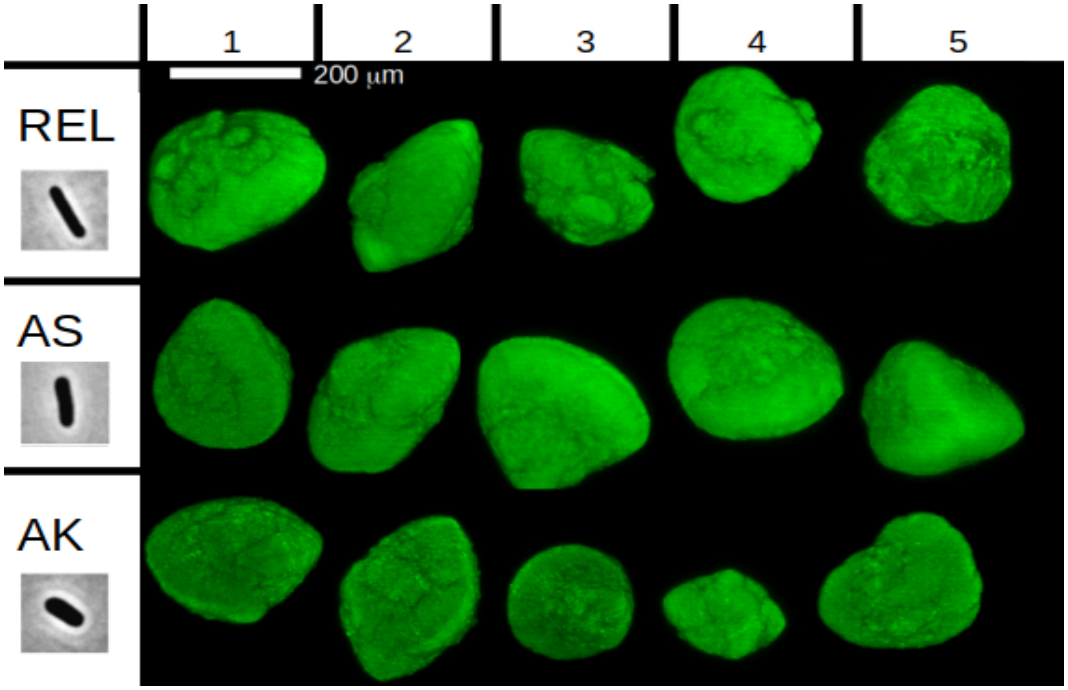


Figure 4.1: Table showing 5 of each strain type REL, AS ad AK, numbered 1-5. Each of the colonies belonging to their respective strain was imaged from the same plate

### Variation of colony shape within plates

Looking a fig 4.1, colonies has shapes that deviates from spherical shapes. REL2, AS2 and AK2 has one of its two axis that is significantly longer than the other with pointed ends, this shape shall be referred to as "rugby shaped". Where as AS4 and AK3 looks more spherical, colonies such as AS1 and REL3 looks to be an intermediate shape between a sphere and a rugby shape, this shape shall be refered to as "egg shaped". Generally the colony shape within the plate is able to vary from ruby shaped, AK2, to spherical, AK3. Mitchell and Wimpenny [24] found that the rugby shaped colony morphology of non motile bacterial strains could be explained by the concentration of agar in the growth medium, they observed that rugby shapes appear at concentrations above 0.65 % agar. Where as colonies grown in concentrations below 0.65% agar were observed to be spherical. From figure 4.1 we see that the colony strains within the same plate of 0.5% agar is able to be both rugby shaped and spherically shaped, indicating that the 0.5% agar concentration used in this experiment where close to some critical agar concentration where colony shape flipped from spherical shapes to rugby shapes and that small fluctuations in agar concentration across the plate could cause the colonies in some regions to become rugby shaped whereas colonies in other regions would become spherical or that other parameters than agar concentration causes the variation in shape observed.

#### Protrusions in the colonies

Colonies REL1, REL2, REL3, REL4 and AS2 all show small protrusions of length $\sim 10 - 20\mu m$ across the protrusions. The constant speed model introduced in section 2.3 predicts that small protrusions in growing fronts can be caused by small hotspots where the growth rate of bacterial located inside the spacial location of the hotspots is higher than the growth rate of bacteria outside the hotspot.

This chapter and the growth models introduced in chapters 5 and 6 will attempt to quantify and explain these observations among other measures of morphology and comparison of the morphology of the three strains REL, AS and AK.

## 4.1 Comparing The Bacterial Strains

### *4.1.1 Aspect Ratio*

The aspect ratio of all colonies was measured, figure 4.2 shows box plots and histograms of each of the three strains, to calculate aspect ratio the average run length in X and Y, AXRL and ARYL where calculated, since the orientation of the colony in the XY plane is determined by the orientation of the plate when imaging, aspect ratio was calculated by always dividing the greatest of the two measured run lengths with the smallest one, causing the aspect ratio of the colony to always be greater than 1.00.

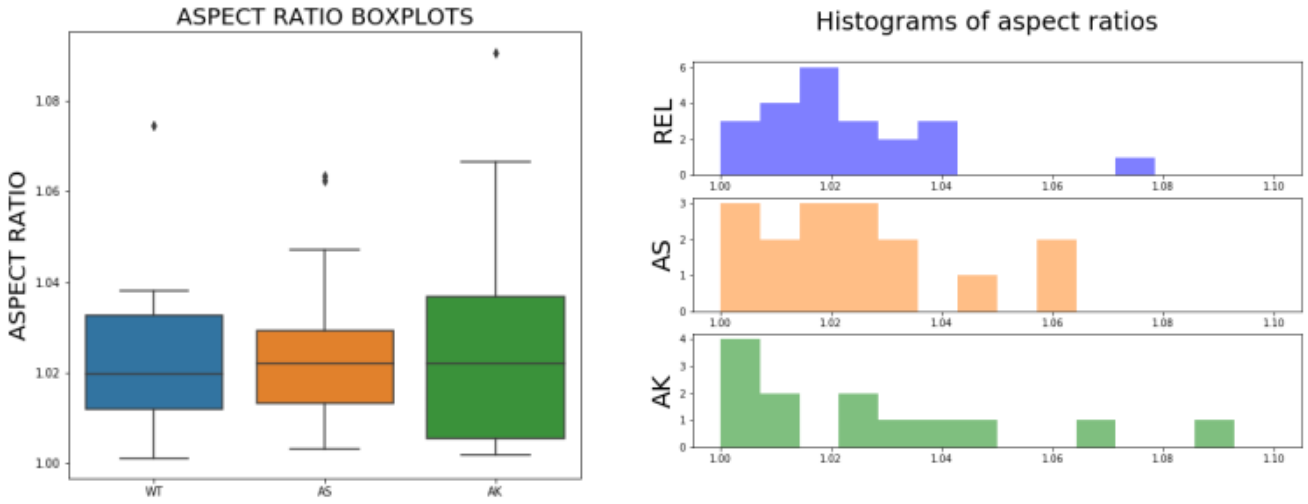


Figure 4.2: **left:** Box plots of aspect ratios of strains REL, AS and AK. **right:** Histograms of aspect ratios of each of the strains

Aspect ratios of the colonies vary from was measured to be in a range between 1.00 and 1.10, to illustrate how colony morphology changes with aspect ratio fig 4.3 show maximum intensity image in the XY plane 5 different colonies labeled A, B, C, D and E with measured aspect ratios of 1.09, 1.07, 1.04, 1.02 and 1.00 respectively. Colonies of 1.00 are spherical or symmetrical E, as aspect ratio increases the colony becomes more egg shaped D and C. As aspect ratio increases above ~ 1.05 the colony becomes rugby shaped and A.

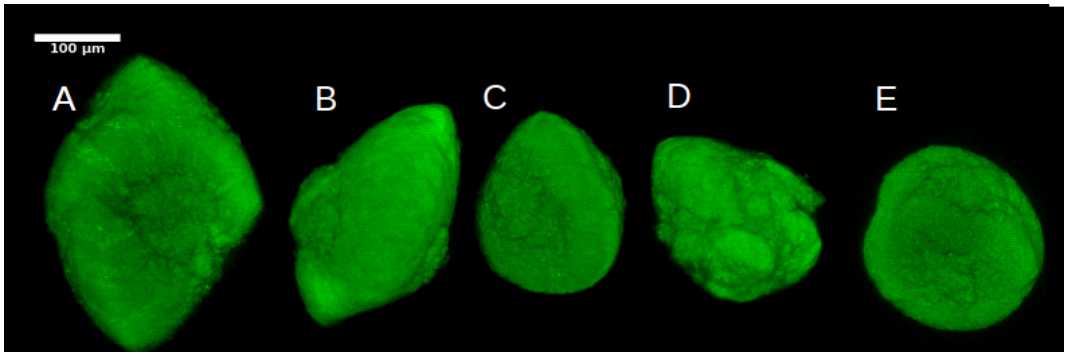


Figure 4.3: 5 colonies with decreasing aspect ratios: Colony A = 1.09, Colony B = 1.07, Colony C = 1.04, Colony D = 1.02, Colony E = 1.00.

ANOVA between the three strain types gives an F-statistic of $F = 0.228$ with a total of 51 colonies analyzed and 3 different strain types comparing to an F-distrubution with 2 and 48 degrees of freedom gives a p-value of $p = 0.797$ comparing with a significace level of $\alpha = 0.05$ the variation of aspect ratios between the strain types is not significant enough to a level where we reject the null-hypothesis that all the strains are similar. Therefore colony aspect ratio is not significantly affected by the individual aspect ratios of the bacteria.

### 4.1.2 Fractal Dimension

Box plots and Histograms of fractal dimension for each of the strains can be seen in figure 4.4. ANOVA of the measured fractal dimensions between the three strains gives an F statistic of $F = 0.241$, comparing the F-distribution with 2 and 48 degrees of freedom this gives a p-value $p = 0.787$ the measured fractal dimesions of the colonies are not statistically significant with the resolution of the surface provided by the Leica N Plan L 40x/0.55na DRY objective .

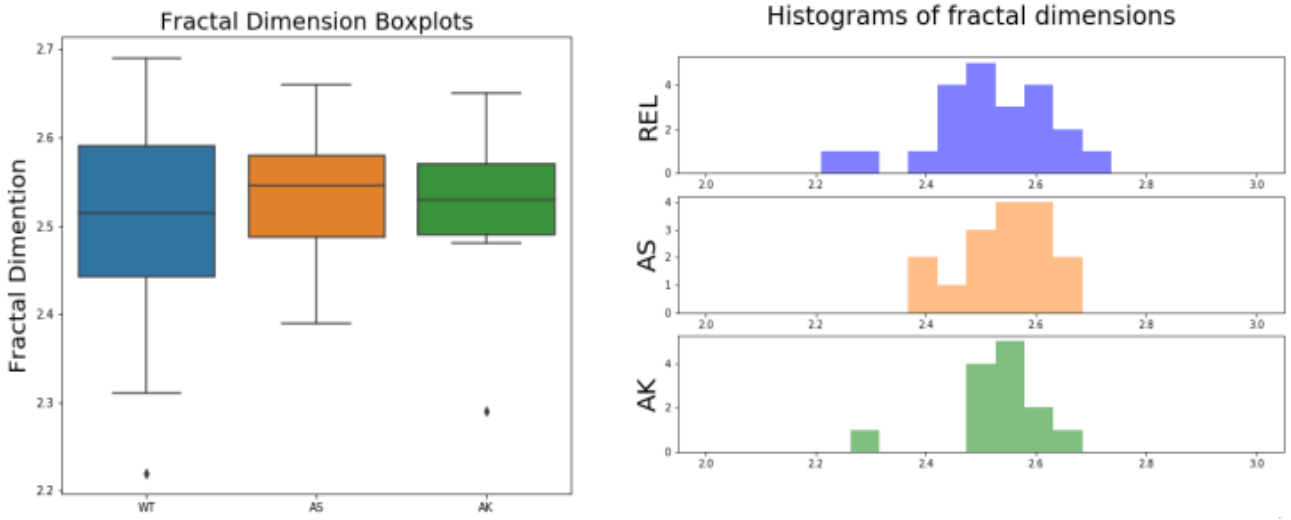


Figure 4.4: **left:** Box plots of measured Fractal Dimension of strains REL, AS and AK. **right:** Histograms of measured Fractal Dimension of each of the strains

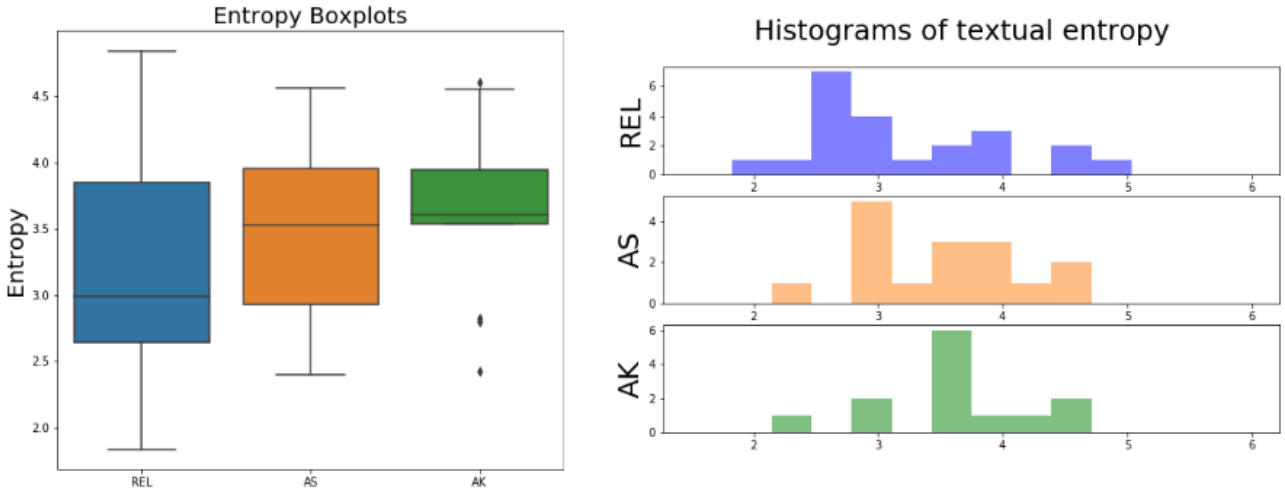


Figure 4.5: **left:** Box plots of measured Textual Entropy of strains REL, AS and AK. **right:** Histograms of measured Textual Energy of each of the strains

### 4.1.3 Textual Entropy

Boxplots and histograms of the Textual Entropy measured on the colonies can be seen in figure 4.5. ANOVA between strains gives an F-statistic of 1.348 which when comparing to F-distribution with 2 and 48 degrees of freedom correspond to a p-value of $p = 0.269$. Measured differences in textual entropy is not statistically significant.

| Strains | degrees of freedom $(N_1 - 1) + (N_2 - 1)$ | t-score | p-value |
|---|---|---|---|
| REL/AS | 36 | 2.7145 | 0.0101 |
| REL/AK | 33 | 2.8621 | 0.007 |
| AS/AK | 27 | 0.4794 | 0.6355 |

Figure 4.6: Statistical comparison of differences in measured textual energy between the three strains. Show that to a significance level of $\alpha = 0.05$ the measured difference in textual energy in the REL strain is significantly different from textual energy measured in AS and AK

### 4.1.4 Textual Homogeneity

Boxplots and histograms of the Textual Homogeneity measured on the colonies can be seen in 4.7. ANOVA between strains gives an F-statistic of 1.348 which correspond to a p-value of $p = 0.058$. Measured differences in textual homogeneity is not statistically significant, to a 5% significance level $\alpha = 0.05$.

### 4.1.5 Textual Energy

Boxplots and histograms of the Textual Energy measured on the colonies can be seen in 4.8. ANOVA between strains gives an F-statistic of 5.759 which correspond to a p-value of $p = 0.0058$. Measured differences in Textual Energy is statistically significant, to a 5% significance level = 0.05. To see where between the three groups differences where significant T-test between the three strains AK, AS and REL, where t-scores between two groups are calculated as:

$$t = \frac{\mu_1 - \mu_2}{\sqrt{\frac{\sigma_1^2}{N_1} + \frac{\sigma_2^2}{N_2}}} \tag{4.3}$$

where $\mu_i$, $\sigma_i$ and $N_i$ are mean, sample standard deviation and number of measurements in group $i$. T-scores between groups and p-values from comparing the t-scores to a two-tailed t-distribution can be seen in table 4.6. Statistical comparison between groups show that to a significance level of $\alpha = 0.05$ the measured differences in textual energy of the REL strain is significantly different than the textual energy measured in the AS and AK strains.

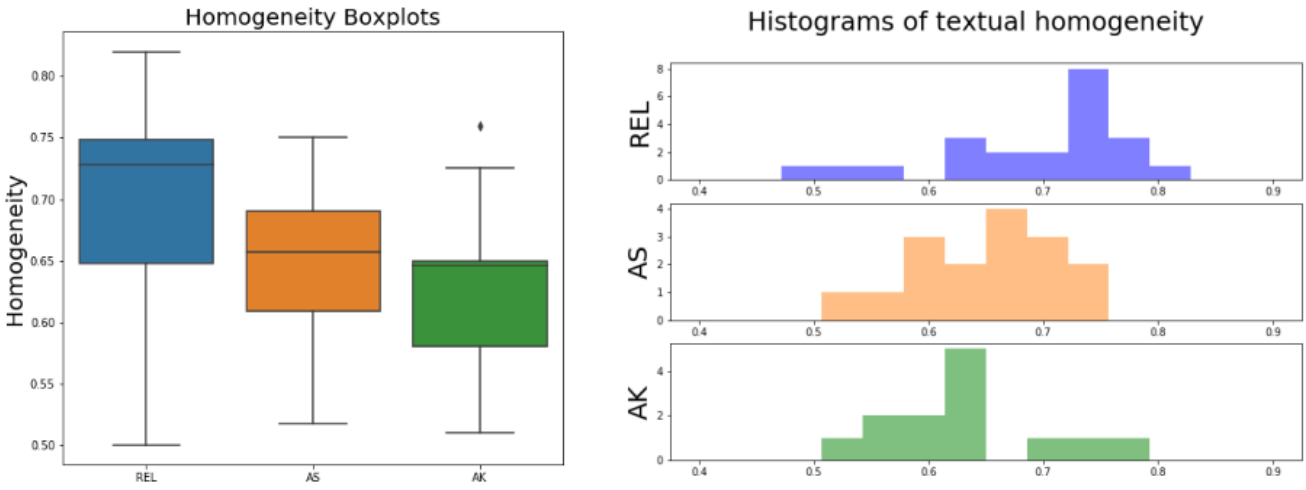


Figure 4.7: **left:** Box plots of measured Textual Homogeneity of strains REL, AS and AK. **right:** Histograms of measured Textual Homogeneity of each of the strains

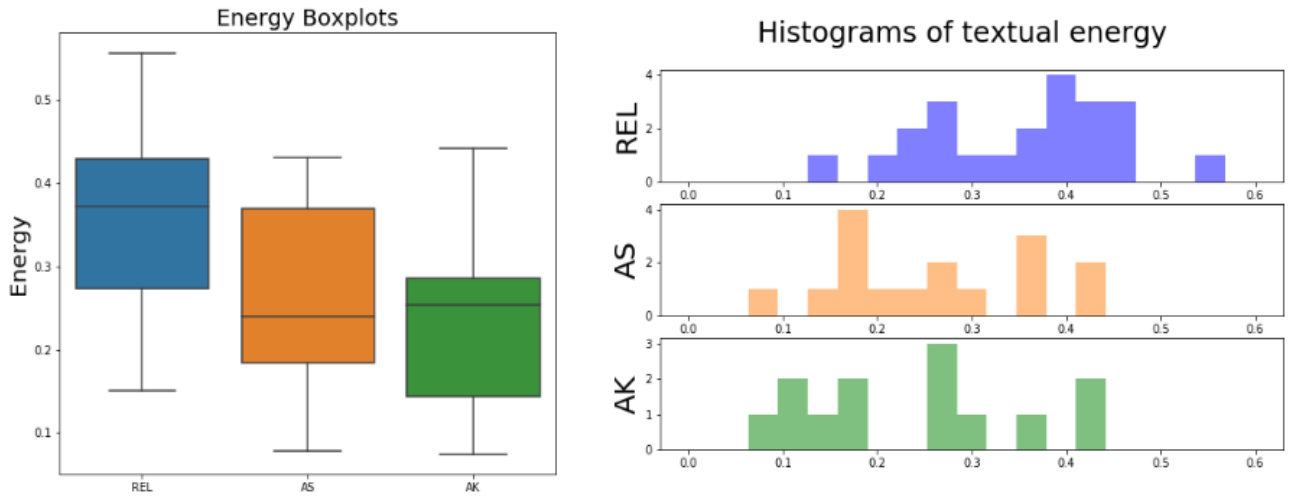


Figure 4.8: **left:** Box plots of measured Textual Energy of strains REL, AS and AK. **right:** Histograms of measured Textual Energy of each of the strains

### 4.1.6 Discussion

The Textual Energy of the REL colonies where measured to be significantly different than the AS and AK colonies, meaning that the images of REL colonies are more homogeneous in the sense that a frequent repeating pattern of pixels within the colony. The Textual Homogeneity measured did not show the same statistically significant difference, despite also being a

measure of homogeneity. This would imply that there is large differences between pixel values in the repeating pixel patterns measured by Textual Energy, since large differences in pixel values contributes less to increase the Textual Homogeneity. This larger measured homogeneity in the REL strain measured in by the Textual Energy could be caused by a tighter packing of the longer rod shaped bacteria than the increasingly more spherically shaped AS, AK all tough this same difference was not measured between AS and AK colonies despite AS strain being a longer rod shape relatively compared to the AK strain.

No significant differences in the colony shape quantified Aspect Ratio where measured between strains. Despite observing varying colony shapes as seen in figure 4.1, these differences in shape where not measured to be related to the individual bacterial shape, indicating that the variation in colony shape could be determined more by local environment of the colonies such as nutrient concentration or the concentration in agar as measured by Mitcell and Wimpenny [24].

No significant differences in fractal dimension were measured, this could be due to the resolution of the 40x/0.55na objective used to image the colonies. Using equation (2.30) the smallest features that can be resolved laterally, with the wavelenght of the green emission lights wavelength being 510nm, is:

$$R_{xy} = \frac{1.22\lambda}{2NA} = \frac{1.22 * 510nm}{2 * 0.55} = 565.63nm$$

Instead switching to 63x/1.20na objective would allow the lateral resolution to more than double

$$R_{xy} = \frac{1.22\lambda}{2NA} = \frac{1.22 * 510nm}{2 * 1.20} = 259.25nm$$

Figure 4.9 show the diffrences in resolved surface structure between an 3D image of a colony taken with the Leica N Plan L 40x/0.55na DRY and the HC PL APO 63x/1,20na W CORR CS2 objective, which visually shows a clear diffrence in the resolution of the surface, therefore a set of images using the 63x/1.20na objective were taken to closer analyze the surface structure of the bacteria. However since a higher resolution due to a larger NA comes with the tradeoff of having to move the objective closer to the sample as explained in section 2.4.2 only the very bottom of the colonies could be consistently imaged therefore only the fractal dimension were measured on these images.

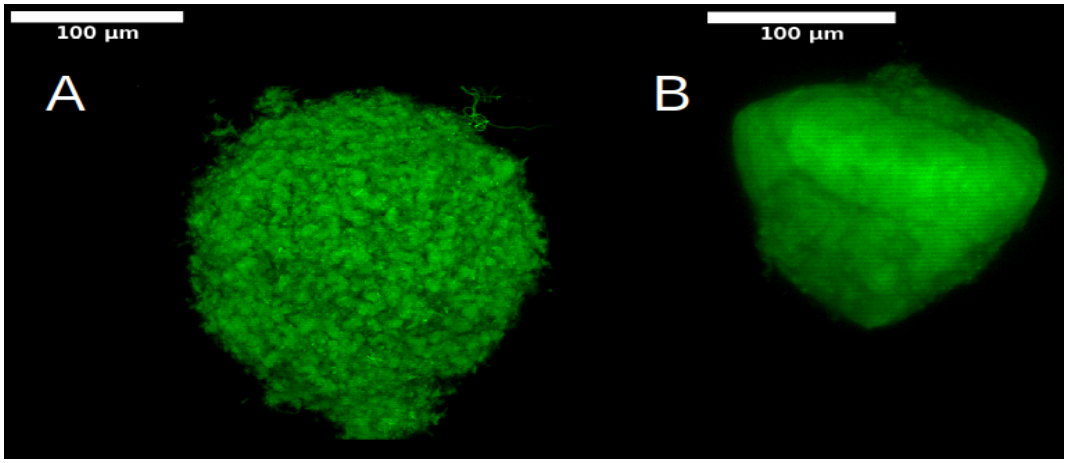


Figure 4.9: **A**: Image of a colony taken using the HC PL APO 63x/1,20na W CORR CS2 objective **B**: image of colony taken using the Leica N Plan L 40x/0.55na DRY objective

## 4.2 Closer Analysis Of The Surface Structure

All images taken with the HC PL APO 63x/1,20na W CORR CS2 objective is available at ERDA following the link [25]. 3D Images of the colonies where taken on three separate days, on day 1 colonies from a plate AS strains and a plate of REL strains where imaged, on day 2 colonies from plates of AS and AK strains where measured and on day 3 colonies from plates of each of the three strains where measured. On days 1 and 2 no AK and REL strains where measured respectively, this was due to no colonies grown in their respective plates where within range of imaging for the 63x/1.20na obective. Ranges of measured fractal dimension ranges from 2.51 at the highest and 2.11 at the lowest. To compare the visual difference between a strain with a large fractal dimension to one with a lower fractal dimension Figure 4.10 shows the structural difference of an AS colony with a surface fractal dimension of 2.51 and an AS colony with surface fractal dimension 2.24 for comparison, as an example.

Figure 4.11 shows the distribution of fractal dimensions measured on the three strains on different days, it shows a clear pattern of fractal dimension measured on strains from the same plate being highly correlated, but almost no correlation between the fractal dimension measured on colonies from the same strain but grown different days on different plates. ANOVA between strains on the measured Fractal Dimension of all colonies gives an F-score of 1.311, with the total number of colonies being 11 of the AS strain, 9 of the AK strain and 8 of the REL strain comparing to an F-distribution with 2 and 25 degrees of freedom this gives a p-value of $p = 0.2874$. This means that there

is no significant difference in the surface structure between all the strains imaged wit the 63x/1.20na objective. However, ANOVA between the three AS plates measured on different days gives an F-score of 9.82 comparing to an F-distribution with 2 and 8 degrees of freedom this gives a p-value of $p = 0.007$ which to a significance level of $\alpha = 0.05$ the hypothesis that plates all with AS strains but grown in different plates are the same. Similarly t-testing between the two REL plates and the two AK plates gives p-values of $p = 0.0001$ and $p = 0.084$ which means that to a significance level of $\alpha = 0.05$ REL plates were measurably different, while the AK plates where not.

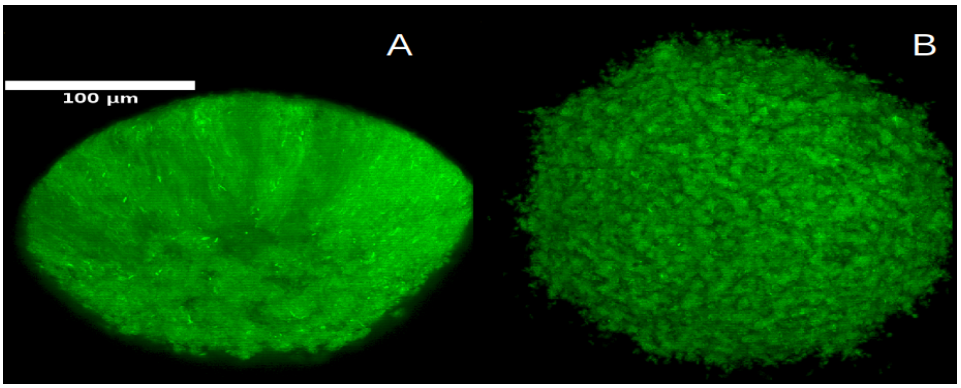


Figure 4.10: Comparison between **A** a AS colony with surface fractal dimension of 2.24 and **B** a AS colony with fractal dimension of 2.51. Imaged with 63x/1.20na objective

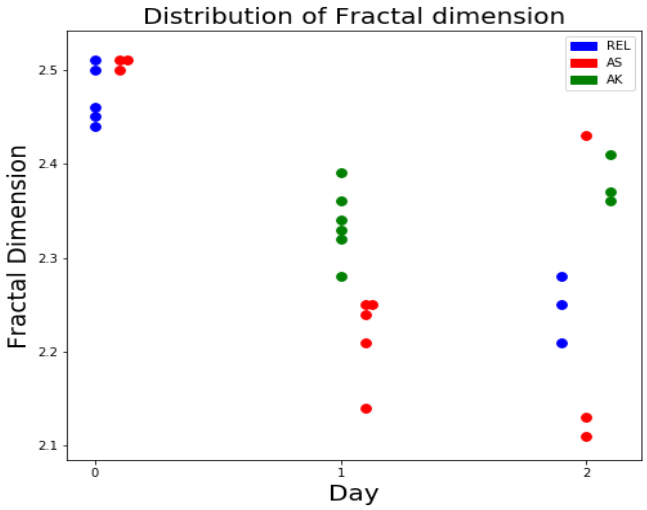


Figure 4.11: Distribution of Fractal Dimensions measured of different days, shows clear difference between individual plates, but none between REL, AS and AK strains

### 4.2.1 discussion

Using the HC PL APO 63x/1,20na W CORR CS2 objective gave sharper images of the colony surfaces, but no statistically significant differences where measured between strains, differences between plates where however measured between different plates of different strains, similarly to the variation of colony shape within plates when imaged with the Leica N Plan L 40x/0.55na DRY objective no difference was found between the three strain. Once again indicating that variation in colony shape is determined by variation the in environment of the colony has much greater measurable effect on colony shape than the individual cell shape, both on a surface level and when measuring colony aspect ratio.

Chapter 5

# Lattice Models

I this chapter the lattice models used to model bacterial growth will be introduced and explained. The basis for all lattice models will be the Eden Growth model, several modifications and additional growth rules will be added to the Eden Growth Model to model the phenomena observed in the real life experiments.

## 5.1 Basic Eden Model

The Eden Model has already been described here an algorithm to implement both version A and version B of the Eden Model as described in section 2.1.1. Both models have been shown to be in the same universality class [5].

### *5.1.1 Version A*

Version A defines the surface of the Eden cluster to be the adjacent unoccupied surface sites. It can be implemented with the following algorithm:

Let L be a 3D lattice. For a site in the lattice $L(i, j, k)$, if $L(i, j, k) = 0$ the site is considered empty and if $L(i, j, k) = 1$ the site is considered occupied by a bacteria:

**Step 1**

Define the initial state of the lattice, to be an empty lattice with a single occupied seed in the middle of the lattice.

**Step 2**

For the lattice state, define the surface of the bacterial colony, $S$, to be all empty sites neighbouring an occupied site. Where the 6 neighbouring sites of a site in the lattice $L(i, j, k)$ is $L(i \pm 1, j, k)$, $L(i, j \pm 1, k)$ and $L(i, j, k \pm 1)$.

**Step 3**

Chose a random surface site $S(i', j', k')$ and update the lattice by setting $L(i', j', k') = 1$.

**Step 4**

Update the surface, by removing the randomly chosen surface site $S(i', j', k')$ from the surface and add to the surface any empty sites neighbouring the randomly chosen site.

**Step 5**

repeat steps 3 and 5

### 5.1.2 Version B

Version B defines the surface to be any occupied site with at least one adjacent unoccupied neighbouring site. This version of the Eden model can be implemented with the following algorithm:
Let L be a 3D lattice. For a site in the lattice $L(i, j, k)$, if $L(i, j, k) = 0$ the site is considered empty and if $L(i, j, k) = 1$ the site is considered occupied by a bacteria:

**Step 1**

Define the initial state of the lattice to be an empty lattice with a single occupied seed in the middle of the lattice.

**Step 2**

For a state in the lattice, let the surface $S$ be the subset of sites that is both occupied by a bacteria and has 1 or more neighbouring empty sites. Where the 6 neighbouring sites of a site in the lattice $L(i, j, k)$ is $L(i \pm 1, j, k)$, $L(i, j \pm 1, k)$ and $L(i, j, k \pm 1)$.

**Step 3**

Randomly select a surface site S(i',j',k').

**Step 4**

This site may have one or several unoccupied neighbours. Randomly select one of the unoccupied sites neighbouring $S(i', j', k')$. Call this randomly selected site $L(a, b, c)$

**Step 5**

Update the Eden cluster by setting $L(a, b, c) = 1$

**Step 6**

If the newly grown to site $L(a, b, c)$ has one or more unoccupied neighbours update the surface S by adding $L(a, b, c)$ to the surface.

**Step 7**

For each of the 6 neighbours $N(i, j, k)$ to $L(a, b, c)$. These sites may or may not be occupied. If they are occupied then they would have been considered surface sites before $L(a, b, c)$ became occupied in step 5. However, due to $L(a, b, c)$ becoming occupied, these site may no longer have an unoccupied neighbours, if that is the case then they would no longer be considered surface sites. Therefore update the surface by doing the following for each of the Neighbouring sites $N(i, j, k)$

**Step 7.1**

Check if $N(i, j, k)$ is occupied.

**Step 7.2**

If they are occupied check if they have at least one unoccupied neighbour site.

**Step 7.3**

If $N(i, j, k)$ is occupied but does not have an occupied neighbour, remove this site from the surface

**Step 8**

Repeat steps 3-8

## 5.2 Time in the Eden Model

When analyzing the Eden model it is useful to have a measure of time, if one bacteria grows with time intervals $\tau$ then the time between growth events for colonies of $N$ bacteria would happen on average with $t = \frac{\tau}{N}$ intervals. In the Eden model only the bacteria located on the surface on the cluster can grow, since the surface in version B is defined as exactly the subset surface sites the has an unoccupied neighbour an therefore can grow it is very natural to measure the time between events in a Eden cluster with N surface sites, $\delta t$, to be:

$$\delta t = \frac{\tau}{N} \longrightarrow \frac{1}{N}, \text{ for } \tau = 1 \tag{5.1}$$

In version A the surface is not defined by the amount of sites that can grow but rather the amount of sites that can be grown into, therefore eq. 5.1 does not hold in version A. For normal Eden Growth with no additional modifications to growth conditions this discrepancy can be accounted for by measuring time in terms of the radius of the Eden Cluster since the radius of the cluster scales linearly with time [8]. However since it is not a given that this holds when making additional rules of growth, the models discussed in the rest of the chapter will be modified versions of Version B of the Eden Model.

## 5.3 Growth Model With Small Hotspots

The constant speed model described in section 2.3.2 predicts that small hotspots will cause small protrusions in a front moving at constant speed normal to its surface. As the front moves beyond the hotspot the protrusion then spreads out as a sideways parabola shown in figure 2.5. Small protrusions were observed in experiments as shown in figure 4.1, therefore to model bacteria growing on a lattice with small hotspots, let bacteria occupying hotspot sites have higher growth rates, $r_h$, than the growth rates, $r_o$,,of the rest of the Eden Cluster not occupying a hotspot site. Where hotspots are defined as small spherical clusters of connected sites scatted around the lattice. Eden Growth with hotspots can be implemented with the following algorithm:

Let L be a 3D lattice. For a site in the lattice $L(i, j, k)$, if $L(i, j, k) = 0$ the site is considered empty and if $L(i, j, k) = 1$ the site is considered occupied by a bacteria, let $r_o$ be the growth rate of a site outside a hotspot and $r_h$ be the growth rate of a site located within a hotspot, where $r_h > r_o$:

**Step 1**

Define an initial state of the lattice, to be an empty lattice with a single occupied seed in the middle of the lattice. Also define $H(i, j, k)$ a subset of lattice sites belonging to a hotspot cluster

**Step 2**

Let the surface sites $S_o$ be the subset of sites that is both occupied by a bacteria, has 1 or more neighbouring empty sites and is located outside of $H(i, j, k)$. And the surface sites $S_h$ be the subset of sites that is both occupied by a bacteria, has 1 or more unoccupied neighbouring sites and is located inside of $H(i, j, k)$.

**Step 3**

The time between growth events of a the surface sites located outside the Hotspots is $t_o = \frac{1}{N_o r_o}$, and the time between growth events inside the hotspot is $t_h = \frac{1}{N_h r_h}$. Time between any growth event is on average $t = \frac{1}{N_o r_o + N_h r_h}$. Select from which of the two surfaces to grow from by selecting a random number between 0 and 1 p.

$$\text{if: } p < \frac{N_o r_o}{N_o r_o + N_h r_h} \text{ Grow from surface } S_o$$

$$\text{else: Grow from surface } S_h$$

**Step 4**

Randomly select a surface site $S_h(i', j', k')$ or $S_o(i', j', k')$ depending on the choice made in step 3.

**Step 5**

This site may have one or several unoccupied neighbours. Randomly select one of the unoccupied sites neighbouring $S(i', j', k')$. Call this randomly selected site $L(a, b, c)$.

**Step 6**

Update the Eden cluster by setting $L(a, b, c) = 1$

**Step 7**

If the newly grown to site $L(a, b, c)$ has one or more unoccupied neighbours update the surfaces by adding $L(a, b, c)$ to $S_h$ if $L(a, b, c) \in H(i, j, k)$. Otherwise add the newly grown to site to $S_o$.

**Step 8**

Remove any sites adjacent to $L(a, b, c)$ that was part of the surface but o longer has an occupied neighbour similarly to step 7 of Eden Model version B

**Step 9**

Repeat steps 3-9.

## 5.4 Alignment Biased Growth Model

To model the effect of individual cell shape on colony morphology with a lattice model, consider a model where the bacteria has an orientation in space, bacteria placed on the lattice can be oriented along one of the x,y,z-axis, in total three different orientations in space is possible. Rod shaped bacteria has shown a tendency align themselves with the orientation of nearby cells due to a combination of cell division and mechanical interactions between neighbouring bacteria [26] [27]. One could imagine that correlations in alignment between local bacteria could influence the shape of the entire cluster.
To model these phenomena on a lattice without calculating the actual mechanical interactions between all the cells, let instead any site in the cluster have an orientation and a preference towards growing into a site along its orientation, mechanical interactions between neighbouring cells are modelled for by making the newly grown to site try to align its neighbors to its own orientation in space. Such a lattice model can be implemented with the following growth algorithm:

Let $L(i, j, k)$ be a 3 dimensional lattice with $L(i, j, k) = 0$ defined as an empty site, $L(i, j, k) = 1$ defined as a site occupied by a bacteria that is aligned along the x-axis, $L(i, j, k) = 2$ defined as a site occupied by a bacteria that is aligned along the y-axis and $L(i, j, k) = 3$ defined as a site occupied by a bacteria that is aligned along the z-axis

#### Step 1

Define the surface S as the set of occupied sites with one or more unoccupied neighbours sites, where the neighbours of the site $L(i, j, k)$ is defined as the 6 sites $L(i \pm 1, j, k)$, $L(i, j \pm 1, k)$ and $L(i, j, k \pm 1)$.

#### Step 2

Randomly select a surface site

#### Step 3

Check the alignment of the selected surface site.
The site may have up to two unoccupied aligned neighbours and up to four unoccupied unaligned neighbours (fx. if $L(i, j, k) = 1$ the aligned neighbours would be $L(i \pm 1, j, k)$ and the unaligned neighbours would be $L(i, j \pm 1, k)$ and $L(i, j, k \pm 1)$). The Selected site will prefer to grow to a neighbour along its own alignment. However, both of these sites may be occupied.

#### Step 4

Count the number of unoccupied aligned neighbours $N_A$ and number of unoccupied unaligned neighbours $N_U$.

If $N_A > 0$ make decision to grow to aligned neighbour site. If $N_A = 0$ make decision to grow to an unaligned neighbour.

**Step 5**

Depending on the decision taken in step 4 randomly select an unoccupied aligned neighbour or unoccupied unaligned neighbour.

**Step 6**

If in step 4 the decision was to grow to an aligned neighbour site:
Grow the colony by setting the site chosen at step 5 equal to the same value as the value in the ”parent” site chosen at step 2.
If in step 4 the decision was to grow to an unaligned neighbour:
Set the value of the site chosen in step 5 to a random value 1,2 or 3. (ie. set the orientation of the site to a random orientation)

**Step 7**

Change the alignment of any occupied sites neighbouring the site selected in step 5, to have the same alignment as the alignment chosen in step 6.

**Step 8**

Update the surface of the cluster.

**Step 9**

Repeat steps 2 to 9.

Chapter 6

# Lattice Results

In this chapter results from lattice modelling of 3D colonies and the models effect on colony shape and surface will be presented. Results, where possible, will be compared to the results of real 3D dimensional colonies presented in chapter 4.

Estimation of the cell count in the colonies grown experimentally for 15 hours were that the colony size were on the scale of $N = 10^6$ cells. Therefore to model and compare results from lattice modelling to the experimental results, Eden Model clusters were grown to a size of $10^6$ sites being occupied. An Three dimensional Eden cluster of size $10^6$ can be seen in figure 6.1

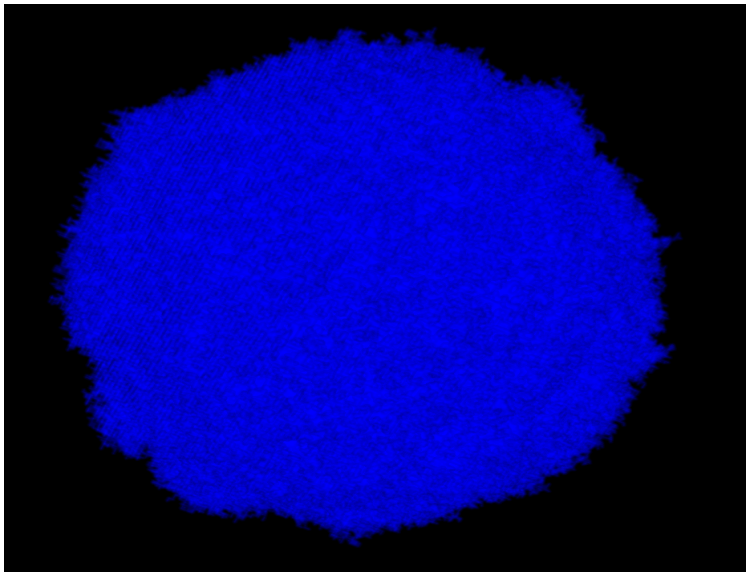

Figure 6.1: Approximately spherical Eden Cluster of size $10^6$ occupieed sites

The Eden Model is approximately spherical with the radius of the cluster increasing linearly with time [8]. Aspect Ratios of the Eden Cluster measured according to equation (2.31) and never increases above 1.01, therefore the basic Eden Model fails to model the range of colony shapes observed experimentally with aspect ratios ranging from 1.00 to 1.10 figure 4.2. In this chapter the Hotspot model described in section 5.3 and the alignment model described in section 5.4 will be tested and their effect on overall colony shape will be measured.

## 6.1 Hotspot Results

The constant speed model for a growing front moving through a hotspot predicts that a small protrusion is craeted on the front as the front moves through the hotspot. In the colonies grown experimentally, shown in figure 4.1, multiple colonies where observed to have protrusions of approximately $10-20\ \mu m$ across. Therefore, in this section a model with a spherical hotspot with a radius of 10 sites. And with the center of the hotspot located 15 sites above the seed in the z-direction of the lattice will be considered. The effects of such a hotspot on the shape of the colony of grown to a size of $10^6$ cells will be considered. Figure 6.2 shows the visual effects of such a hotspot with growth rates inside the hotspot being double the growth rates outside the hotspot.

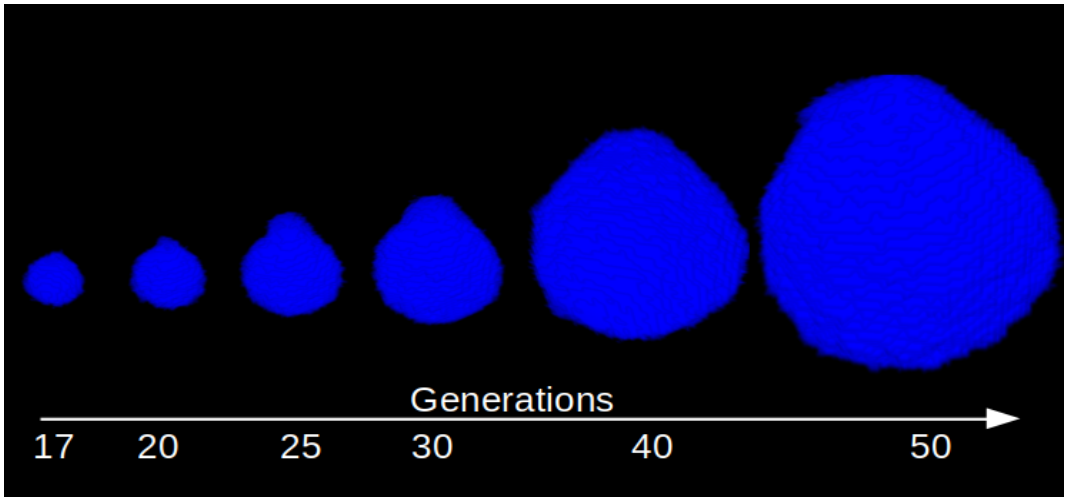


Figure 6.2: Shape of an Eden Growth Cluster growing through a hotspot after $t$ = 17, 20, 25, 30, 40 and 50 generations. The downstream effects of the protrusion growing as the Cluster passes trough the hotspot starting after approximately 15 generations is a slightly eggshaped cluster after 40-50 generations

Figure 6.2 shows a protrusion on the Eden Cluster being formed as the cluster moves through the hotspot between generations 17 and 25. The downstream effect of the protrusion created by the hotspot is a visually slightly egg shaped cluster. Experimentally several egg shaped colonies were observed. Figure 4.3 showed that colonies with an egg shape had a measured aspect ratio of approximately 1.02 to 1.04. To quantify the effect on the aspect ratio of the Eden Cluster growing through a hotspot figure 6.3 shows the aspect ratio as a function of generation time of an Eden Cluster growing through a Hotspot with varying growth rates.

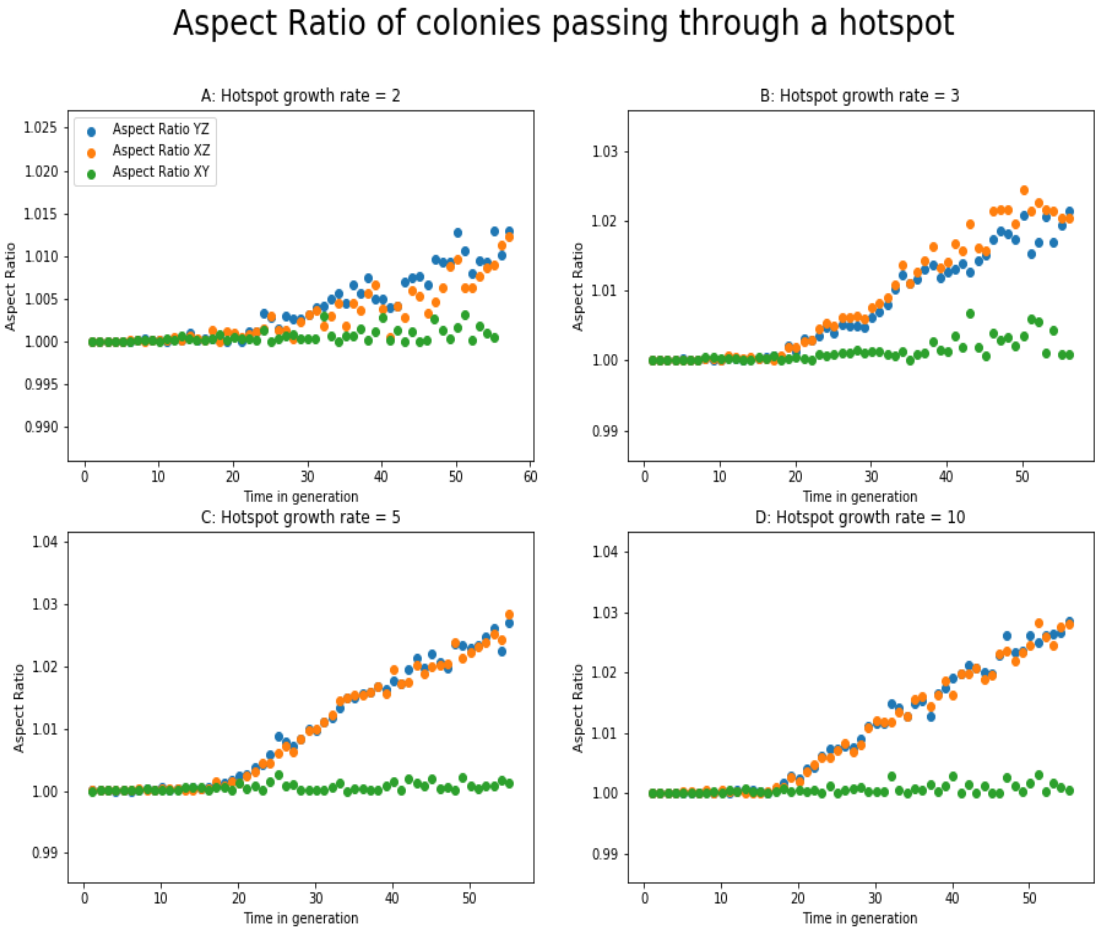


Figure 6.3: Aspect ratios in the XY, XZ and YZ-direction of an Eden Cluster growing through a hotspot, with growth rates $r$ of **A**: $r = 2$, **B**: $r = 3$, **C**: $r = 5$ and **D**: $r = 10$, located with center a distance of 25 sites above the seed of the cluster in the z-direction. For cluster with size of $10^6$ sites the aspect ratios of the cluster in both XZ and YZ-directions is in the egg shaped range between 1.2-1.4 oberserved experimentally

The figure shows that the aspect ratio in the $XZ$ and $YZ$ directions of the cluster increases with time as the cluster grows through the hotspot and for hotspot growth rates between 3 and 10 times larger than growth rates outside the hotspot increases the aspect ratio of the colony to values between 1.02 and 1.04 for clusters of size $10^6$, similarly to the aspect ratios of egg shaped colonies observed experimentally.

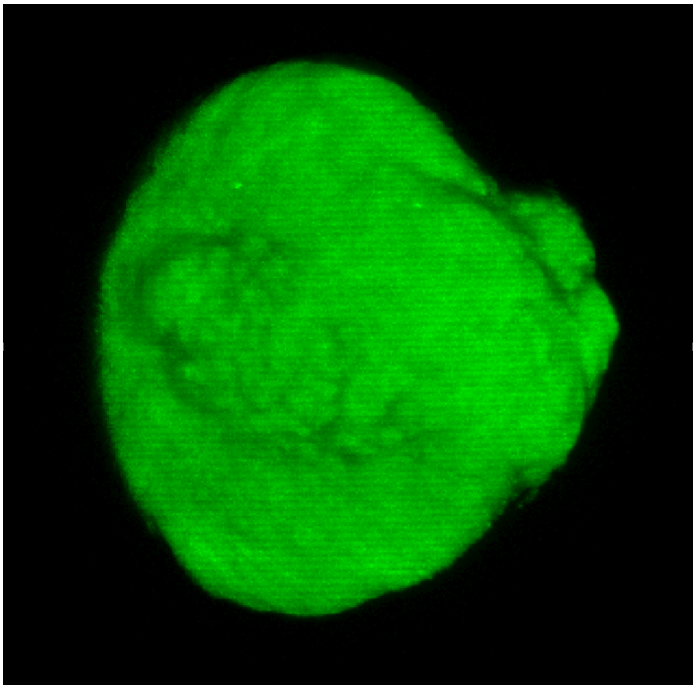

Figure 6.4: REL colony imaged with 40x/0.55na objective with visible protrusions, lattice modelling of surface growth of colonies single protrusions predicts the colony to become egg shaped if continued growing

**Discussion**

A lattice model containing small hotspots show at least the ability to replicate some of the shapes of the colonies seen experimentally, showing that a single hotspot will cause the shape of the colony downstream to be egg shaped. The question is then if the protrusions and egg shapes were actually due to colony growing through a hotspot spot or not. One could speculate that the solid 0.5% agar and minimal media contained a heterogeneous distribution of nutrients which could cause bacteria in some areas of the agar to have more nutrients available to them and therefore have an increased growth rate locally. However, without any testing of the nutrient distribution in the plates, this remains speculative. It should be noted that the dynamics of the Eden Model after it has passed through a hotspot is independent on the hotspot itself only on the shape of the perturbation caused by the hotspot. In that sense the spreading out from the protrusion causing the

cluster to become egg shaped is only a consequence by the normal surface growth of the Eden Model, not by a variation in growth rates induced by the hotspot. Therefore the effect of any protrusion on the length scale tested here, whether caused by a hotspot or not, will have the downstream effect on the colony that it becomes egg shaped. Figure 6.4 shows an example of an experimentally observed colony with small protrusions on the surface, while it has proven outside the scope of this thesis to find out what caused these protrusions in the first place, we can with the hotspot lattice model predict what effect these protrusions will have on colony shape if growth is continued, namely that growth of the colony normal to the surface of the protrusions will cause the colony to become egg shaped. It can also be speculated that he egg shaped colonies observed experimentally is a consequence of the colony in earlier times having formed small protrusions, this also remains speculation but could be tested by observing growing colonies using a time lapse microscope. This would allow for tracking of the growth over time as the colony takes shape.

## 6.2 Alignment Lattice Model

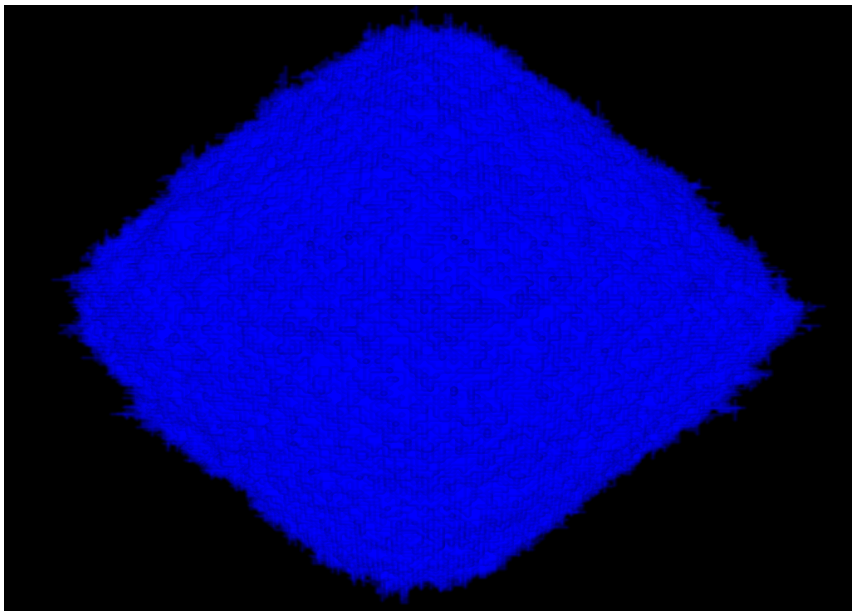

Figure 6.5: Diamond shaped cluster of size $10^6$ cluster sites grown using the Alignment biased model described in section 5.4

Figure 6.5 shows a cluster of size $N = 10^6$ sites occupied, grown using the alignment biased model. The cluster is visibly diamond or bipyramid shaped similarly to clusters grown by M.T. Batchelor and B.I. Henry in [6]

where diamond shaped clusters where found using noise reduction methods while growing large Eden clusters.

The intention of the Alignment Biased Model was to model the varying colony shapes observed experimentally. To test the effects of competition between aligned sites on colony shape figure 6.6 shows measured aspect ratios of 4 Alignment biased clusters showing no significant deviations in aspect ratio away from 1.00 in any direction X, Y and Z, and never approaching the ranges in aspect ratio measured in real 3D colonies that ranged from 1.00 to 1.09

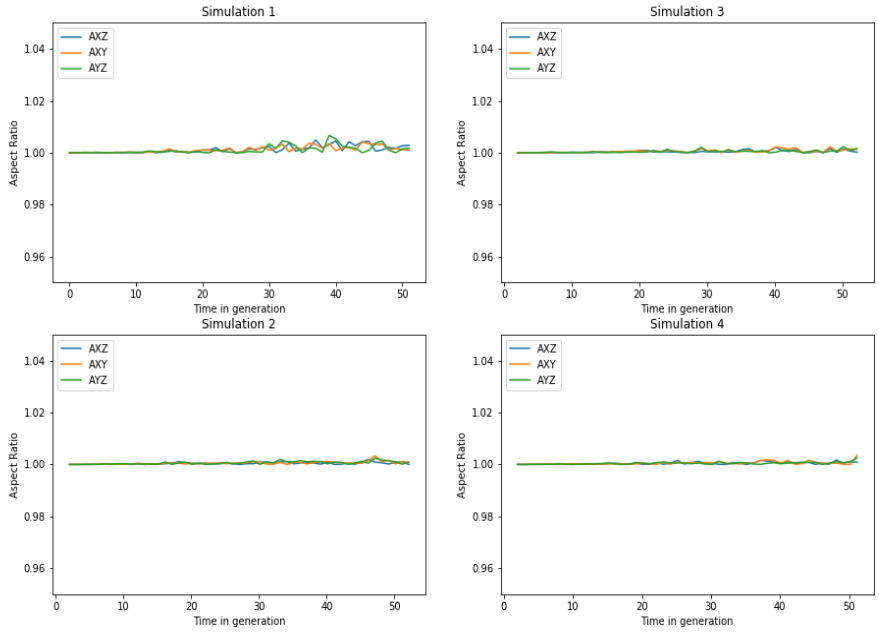


Figure 6.6: Aspect ratio in all directions X,Y and Z over time for 4 clusters shows that the clusters never deviate form symmetrical cluster shapes.

It as he imagination that variation in colony morphology in the Alignment Biased Model was driven by clusters of similarly aligned sites, causing the cluster to distort away from spherical colony, this seems not to be the case. To measure how strong correlations between similarly aligned sites, the probability that two neighbouring points had the same alignments, $C_p$ were calculated . Figure 6.7 shows a cross section view of the alignment model in the xy-plane with sites of color red being aligned in the x-directions, blue sites being aligned in the y-direction and green sites being aligned in the z-direction. For a model with randomly placed alignments $C_p$ would be ex-

pected to be $C_p = 0.33$ since there are three possible alignments for clusters of size $10^6$, $C_p$ was found to be:

$$C_p = 0.4296 \pm 0.0004 \tag{6.1}$$

Showing that any given site is expected to have more than half of its neighbouring sites have a different alignment than itself. Figure 6.7 A also visibly shows that cluster of similarly aligned sites are relatively small compared to the overall cluster and it is unlikely that these clusters could have large scale effects on colony shape.

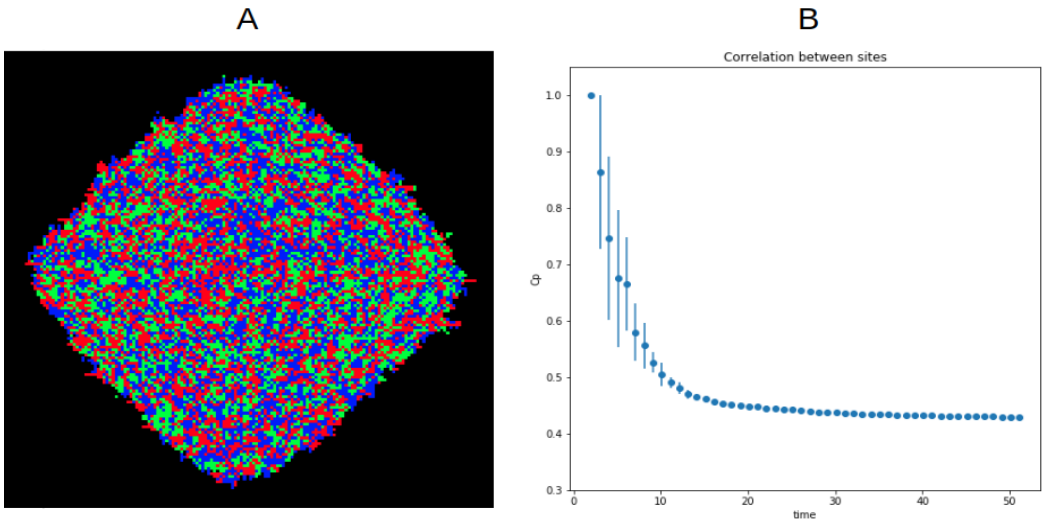


Figure 6.7: **A:** Cross section view of the XY plane of a cluster, red colors is sites aligned in the x-direction, y is sites aligned in the y-direction and green is sites aligned in the z-direction **B:** probability of neighbouring sites sharing alignments as the model grows

### 6.2.1 Comparison to the Eden Model

Here comparison between the scaling exponents and the measured anisotropy between the Eden model and the Alignment Biased Model is made

#### Anisotropy

The Eden model have been measured to be slightly anisotropic along the axes of the lattice, being approximately 2% longer in the directions of the lattice compared to the average distance from the surface to the center of the colony [6]. Here the anisotropy is calculated as the ratio between the distance from the surface to the center along the three axes of the cluster, so in total an average of the six extrema points of the diamond shaped cluster, and the average distance from all the surface sites to the cluster center. An average

anisotropy of four simulations using the alignment model, measuring the anistropy as the model growns can be seen in figure 6.8. The anisotropy, A, of the alignment model of $10^6$ sites is measured to be:

$$A = 1.16 \pm 0.04 \tag{6.2}$$

Significantly larger than the 2% anisotropy for large Eden clusters.

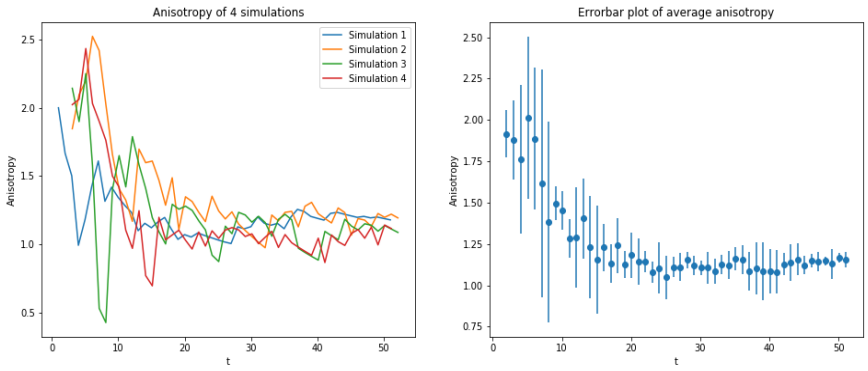


Figure 6.8: **left:** Anisotropy of the cluster of four simulations and **right:** an average of all simulations

### Scaling of the Alignment model

Scaling of the Eden model in radial geometries has found a growth exponent of $\beta = 0.1047 \pm 0.0014$ [8] and the radius of the Eden cluster scales linearly with time, $R \propto t$. Figure 6.9 shows the average cluster radius of four simulations as function of time and a loglog plot of the average width of the clusters as function of time.

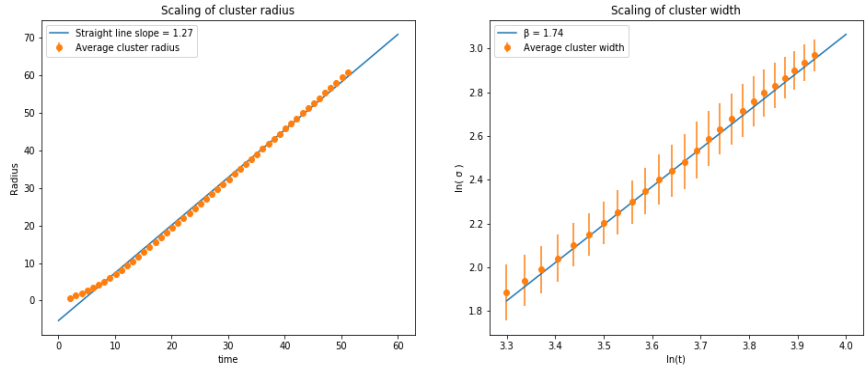


Figure 6.9: **left:** Scaling of radius with time and a line drawn with slope 1.27and **right:** scaling of width with time and a line of slope 1.74 drawn

Fitting a straight line to the radius vs time plot in order to find the slope of the line using the mean radius $\bar{r}$ and standard deviation $s_i$ of the mean radius of the four simulations, the slope of the line was calculated by using the weighted sum of squares according to [21] minimizing:

$$\sum_i \frac{(\bar{r}_i - mt_i - c)^2}{s_i} \tag{6.3}$$

Where m is the slope and c is the intercept of the line, the slope m is found to be:

$$m = 1.270 \pm 0.003 \tag{6.4}$$

Meaning that the radius of the cluster increases with $\sim 1.27$ for every unit of time. Similarly a straight line can be fitted to the log of the mean width of the four simulations $log(\bar{\sigma})$ as a function of the log of the time $log(t)$ using that if the error of the measured $\bar{\sigma}$ is $s$ then the error on $log(\bar{\sigma})$, $\hat{s}$,is:

$$\hat{s} = \frac{s}{\bar{\sigma}} \tag{6.5}$$

Weighted sum of squares can be used, minimizing:

$$\sum_i \frac{(log(\bar{\sigma}_i) - \beta log(t_i) - c)^2}{\hat{s}_i} \tag{6.6}$$

Where $\beta$ is the slope, the width of the Alignment model is found to have scaling exponent:

$$\beta = 1.74 \pm 0.11 \tag{6.7}$$

Which is significantly different form the scaling exponent of the radial Eden model where $\beta = 0.1047 \pm 0.0014$

### 6.2.2 Discussion

The Alignment Biased Model proved to be a poor model for modelling shapes observed experimentally, only amplifying the known anisotropy of the Eden Model leading to diamond shaped but symmetrical colony clusters with aspect ratios of approximately 1. Its likely that modelling the mechanical interactions between cells, that causes cells align themselves within colonies [26] is poorly described by square lattice growth models where the directions of alignment is limited to being along the three axes of the lattice. An individual based model, modelling all the mechanical interactions between cells may prove a more useful tool for modelling the effects of cell alignment on colony shape, such as the spring model described in [28]. Measuring the growth exponent $\beta$ of the Alignment Biased model it was found to have significantly different scaling from the Eden Growth model.

Chapter 7

# Conclusion and Outlook

## 7.1 Conclusion

Experimental results showed bacterial colonies of a variety of shapes ranging from spherical to rugby shaped. Characterizing the colony in terms of aspect ratio equation (2.31) it was found that colonies of spherical, egg and rugby shape could appear within the same plates, where growth conditions could be presumed to be close to identical. Comparing the shape of three different strains each with different aspect ratios, no statistical significant difference in colony shape characterized by aspect ratio were found between strains. Previous work by Mitchell and Wimpenny [24] suggests that the rugby shaped colonies of non-motile bacterial strain appears with higher concentrations of agar above 0.65% indicating that fluctuations in agar concentration within the plate could be responsible for the appearance of rugby shaped colonies. Some of the observed colonies displayed small protrusions of approximately $10-20\ \mu m$ in size, the constant speed model and lattice experiments predicts that protrusions of this size on the colony size scales of $10^6$ cells could cause the colony shape to become egg shaped with aspect ratios of approximately $1.02-1.04$. A high resolution look at the colony surfaces, varying in roughness, shown in is 4.10. Quantifying the surface texture by measuring the fractal dimension of the surfaces, showed no statistical difference between the fractal dimension of colonies grown from different strains but significant differences between plates. Lattice modelling of individual cell shape failed to predict the colony shapes seen experimentally. Instead, the Alignment Biased Model exaggerated the known anisotropy of the Eden Model, proving to be a poor model for predicting 3D bacterial growth. All this evidence suggests that environmental effects on colony shape where much greater than the effects of individual cell shape. And that the random fluctuations

in nutrients and agar density within the experimental setup, both between and within plates had a more significant effect on colony shape and surface than the cell morphology.
Differences in the Textual Energy between strains, were found to statistical significance between the wild type strain REL and its two mutant strains AS, AK but no significant difference were found between AS and AK. Textual Energy is a homogeneity measure, quantifying the frequency of repeating pixel patterns in the 3D grey scale images of the colonies. Its can be speculated that difference in Textual Energy comes from a tighter packing of rod shaped bacteria compared to the shorter more spherically shaped AS and AK strains. Since less space between neighbouring cells could lead to more regular pixel patterns. Although without a imaging resolution allowing for separation of individual cells this remains speculation.

## 7.2 Outlook

The experimental setup used in this thesis proved to have fluctuations in the environmental conditions of the bacterial strains that out weighted the effects of individual cell shapes on colony morphology, the next step in the experimental setup would be to better control for nutritional and agar concentration variations which proved to significantly effect colony morphology. Modelling of hotspots and their effect on colony morphology showed that they could explain the egg shaped colony shape arising from small local protrusions in the colony shape, imaging methods such as time lapse microscopy tracking the growth and formation of an egg shaped colony over time would be able to test this hypothesis. Modelling of individual shape on a lattice proved to give results inconsistent with experimentally grown colonies. An individual based model simulating the precise mechanical interactions between cells may prove more useful to understand the effect of individual cell shape on colony growth. Finally imaging methods allowing for detection of single cells may help illuminate the reasons for the measured differences in Textual Energy between strains.

Chapter 8

# Appendices

## 8.1 Intersections between two circles

For two circles with centers located 2w apart along the x-axis with radius d, let circle A have center in $(x_1, y_1) = (w, 0)$ and circle B have center in $(x_2, y_2) = (-w, 0)$ The equation for circle A is then:

$$(x - w)^2 + y^2 = d^2 \tag{8.1}$$

and for circle B the equation is

$$(x + w)^2 + y^2 = d^2 \tag{8.2}$$

To find the points of intersection equate the two equations

$$(x - w)^2 + y^2 - d^2 = (x + w)^2 + y^2 - d^2 \tag{8.3}$$

$$4wx = 0 \tag{8.4}$$

$$x = 0 \tag{8.5}$$

$$w^2 + y^2 = d^2 \tag{8.6}$$

$$y^2 = d^2 - w^2 \tag{8.7}$$

$$y^2 = d^2(1 - \frac{w^2}{d^2}) \tag{8.8}$$

$$y = \pm d\sqrt{1 - \frac{w^2}{d^2}} \tag{8.9}$$

# Bibliography


[1] M.H.Zwieetering et al. "Modeling of the Bacterial GrowthCurve". In: *Applied and environmental microbiology*, 56.6 (1990), pp. 1875–181. DOI: https://doi.org/10.1128/AEM.56.6.1875-1881.1990.

[2] Masahiro Ohgiwaro et al. "Morphological changes in growth phenomena of bacterial colony patterns". In: *Journal of the phsical society of Japan* 61.3 (1992), pp. 816–822. DOI: https://doi.org/10.1143/JPSJ.61.816.

[3] M. Eden in: "Proceedings of the Fourth Berkeley Symposium on Mathematical Statistics and Probability. Vol. IV: Biology and Problems of Health. Edited by Jerzy Neyman, University of California Press, Berkeley and Los Angeles". In: (1961), pp. 223–239. DOI: https://doi.org/10.1002/bimj.19640060422.

[4] D E Wolff. "Wulff construction and anisotropic surface properties of two-dimensional Eden clusters". In: *Journal of Physics A: Mathematical and General* 20.5 (1986), pp. 1251–1258. DOI: https://doi.org/10.1088/0305-4470/20/5/033.

[5] R. Jullien and R. Botet. "Surface thickness in the Eden model". In: *Physical Review Letters* 54 (1985), pp. 2055–2055. DOI: https://doi.org/10.1103/PhysRevLett.54.2055.

[6] M.T. Batchelor and B.I. Henry. "Limits to Eden growth in two and three dimensions". In: *Physics Letters A* 157.4,5 (1991), pp. 229–236. DOI: https://doi.org/10.1016/0375-9601(91)90057-F.

[7] Albert-Laszlo Barabasi and H. Eugene Stanley. *Fractal Concepts In Surface Growth, Chapter 2*, pp. 20–23.

[8] Eric W Kuennen and C Y Wang. "Off-lattice radial Eden cluster growth in two and three dimensions". In: *Journal of Statistical Mechanics Theory and Experiment* 5 (2008), pp. 1–13. DOI: http://doi.org/10.1088/1742-5468/2008/05/P05014.

[9] Wolfram Möbius, Andrew W. Murray, and David R. Nelson. "How Obstacles Perturb Population Fronts and Alter Their Genetic Structure". In: *PLOS Computational Biology* (2015), pp. 1–30. DOI: https://doi.org/10.1371/journal.pcbi.1004615.

[10] Wolfram Möbius et al. "The collective effect of finite-sized inhomogeneities on the spatial spread of populations in two dimensions". In: *arXiv preprint arXiv:1910.05332* (2019), pp. i–xi. DOI: https://doi.org/10.1371/journal.pcbi.1004615.

[11] Vinod Subramaniam Ankur Jain Christian Blum. *Advances in Biomedical Engineering*, pp. 146–170.

[12] James Jonkman et al. "Tutorial: guidance for quantitative confocal microscopy". In: *Nature Protocols* 15 (2020), pp. 1585–1611. DOI: https://doi.org/10.1038/s41596-020-0313-9.

[13] Haluk Beyenal et al. "Three-dimensional biofilm structure quantification". In: *Journal of Microbiological Methods* 59 (2004), pp. 395–413. DOI: https://doi.org/10.1016/j.mimet.2004.08.003.

[14] Albert-Laszlo Barabasi and H. Eugene Stanley. *Fractal Concepts In Surface Growth, Chapter 3*, pp. 29–37.

[15] Image. *Image of the Sierpinsky Gasket from wikipedia*. URL: https://en.wikipedia.org/wiki/Sierpi\%C5\%84ski_triangle#/media/File:Sierpinski_triangle.svg.

[16] Russell D. Monds et al. "Systematic Perturbation of Cytoskeletal Function Reveals a Linear Scaling Relationship between Cell Geometry and Fitness". In: *Cell Reports* 114.3 (2014), pp. 1528–1537. DOI: https://doi.org/10.1016/j.celrep.2014.10.040.

[17] Lonza. *Lonza pmax cloning vector*. URL: https://bioscience.lonza.com/lonza_bs/CH/en/Transfection/p/000000000000191671/pmaxCloning-Vector.

[18] Implen. *Implen NanoPhotometer usermanual*. URL: https://www.implen.de/wp-content/uploads/docs/User_Manual_V4.2.1_N120_NP8_N60_N50_C40_190819.pdf.

[19] Leica. *HC PL APO 63x/1,20 W CORR CS2*. URL: https://www.leica-microsystems.com/objectivefinder/objective/506356/.

[20] Victoria E. Centonze and John G. White. "Multiphoton Excitation Provides Optical Sections from Deeper withinScattering Specimens than Confocal Imaging". In: *Biophysical Journal* 75 (1998), pp. 2015–2024. DOI: https://doi.org/10.1016/S0006-3495(98)77643-X.

[21] R. J. Barlow. *Statistics: A Guide to the Use of Statistical Methods in the Physical Sciences*.

[22] Leica. *Leica N Plan L 40x/0.55na*. URL: https://spectraservices.com/product/506060.html.

[23] Martin Møller Larsen. *Dataset with 40x/0.55na objective*. URL: https://sid.erda.dk/sharelink/G4FUrSnX94.

[24] A.J. Mitchell and J.W.T. Wimpenny. "The effects of agar concentration on the growth andmorphology of submerged colonies of motile and non-motile bacteria". In: *Journal of Applied Microbiology* 83 (1997), pp. 76–84. DOI: https://doi.org/10.1046/j.1365-2672.1997.00192.x.

[25] Martin Møller Larsen. *Dataset with 63x/1.20na objective*. URL: https://sid.erda.dk/sharelink/hM09JMYtlQ.

[26] Dimitry Volfson et al. "Biomechanical ordering of dense cell populations". In: *PNAS* 105(40) (2008), pp. 15346–15351. DOI: https://doi.org/10.1073/pnas.0706805105.

[27] Denis Boyer et al. "Buckling instability in ordered bacterial colonies". In: *Physical Biology* 8.2 (2011), pp. 1585–1611. DOI: https://doi.org/10.1088/1478-3975/8/2/026008.

[28] James Winkle et al. "MODELING MECHANICAL INTERACTIONS IN GROWING POPULATIONS OF ROD-SHAPED BACTERIA". In: *Physical Biology* 14.5 (2017), pp. 1–13. DOI: https://doi.org/10.1088/1478-3975/aa7bae.